Supporting Information

Biomimetic phage-inspired supramolecular system based on glucose-conjugated pillar[5]arene with ciprofloxacin hydrochloride

Yulia I. Aleksandrova[a], Dmitriy N. Shurpik[a,] Arina V. Pergat[a], Alan A. Akhmedov[a], Olga A. Mostovaya[a], Mikhail S. Bukharov[a], Yulia O. Bukarinova[b], Evgenia V. Subakaeva[c], Evgeniya A. Sokolova[b] and Ivan I. Stoikov[a,]**

a Kazan Federal University, A.M. Butlerov Chemistry Institute, 420008 Kremlevskaya, 18, Kazan, Russian Federation

b Kazan Federal University, Institute of Ecology, Biotechnology and Nature Management, 420008 Kremlevskaya, 18, Kazan, Russian Federation

c Kazan Federal University, Institute of Fundamental Medicine and Biology, 420008 Kremlevskaya, 18, Kazan, Russian Federation

***Corresponding Author**
E-mail: dnshurpik@mail.ru (D.N. Shurpik), Ivan.Stoikov@mail.ru (I.I. Stoikov),
Tel.: +7-8432-337463

Electronic Supplementary Information (30 pages)

1. Materials and methods

Materials

Most chemicals were purchased from Merck and used as received without additional purification. Organic solvents were purified in accordance with standard procedures. Dimethylformamide (Merck), 1-thio-β-D-glucose tetraacetate (Merck), dichloromethane (Merck), methanol (Merck), sodium methylate (Merck), lomefloxacin hydrochloride (Merck), norfloxacin hydrochloride (Merck), moxifloxacin hydrochloride (Merck), ciprofloxacin hydrochloride (Merck), $CDCl_3$ (Merck), D_2O (Merck).

Pillar[5]arene **1** was synthesized according to the literature procedure.[S1]

Methods

^1H NMR, ^{13}C NMR spectra were obtained on the Bruker Avance-400 spectrometer ($^{13}C\{^1H\}$ − 100 MHz and ^1H and 2D NOESY - 400 MHz − 400 MHz). Chemical shifts were determined against the signals of residual protons of deuterated solvent ($CDCl_3$, D_2O). The concentration of the sample solutions was 3–5%.

Attenuated total internal reflectance IR spectra were recorded with Spectrum 400 (Perkin Elmer) Fourier spectrometer. The IR spectra from 4000 to 400 cm^{-1} were considered in this analysis. The spectra were measured with 1 cm^{-1} resolution and 64 scans co-addition.

Elemental analysis was performed with Perkin Elmer 2400 Series II instrument.

Melting points were determined using a Boetius Block apparatus.

Mass spectra (MALDI-TOF) were recorded on the Ultraflex III mass spectrometer in the 4-nitroaniline matrix. **Electrospray ionization mass spectra (ESI)** were obtained on the AmazonX mass spectrometer (Bruker Daltonik GmbH, Bremen, Germany). Measurements were carried out in the regime of positive ions registration in the m/z range from 100 to 2800. The voltage on the capillary was 4500 V. Nitrogen was used as the gas-drier with the temperature of 300 ºC and the flow rate of 10 $L \cdot min^{-1}$. The compounds were dissolved in acetonitrile to the concentration of 1×10^{-6} g/L. Data was processed using DataAnalysis 4.0 (Bruker Daltonik GmbH, Bremen, Germany).

Additional control of the purity of the compounds and monitoring of the reaction were carried out by the thin-layer chromatography using Silica G, 200 μm plates, UV 254.

Dynamic light scattering (DLS). The particle size and zeta potential were determined by the Zetasizer Nano ZS instrument at 20 ºC. The instrument contains 4mW He-Ne laser operating at a wave length of 633 nm and incorporated noninvasive backscatter optics (NIBS). The measurements were performed at the detection angle of 173º and the software automatically determined the measurement position within the quartz cuvette. The 1×10^{-3} – 1×10^{-6} M of the **3**, Cipro and **3** with Cipro in H_2O were prepared.

Electrophoretic mobility of different samples was determined using a fold capillary cuvette (Folded Capillary Cell DTS1060, Malvern, U.K.). The experiments were carried out for each solution in triplicate.

Preparation of lipid vesicles. To prepare stock lipid suspensions, mixture of 16.2 mg + 1.9 mg 1,2-dipalmitoyl-sn-glycero-3-phosphocholine (Avanti Polar Lipids, Birmingham, AL, USA) + 1-palmitoyl-2-oleoyl-sn-glycero-3-phospho-(1′-rac-glycerol) (sodium salt) was placed in flat bottom beaker and dissolved in 500 μL of chloroform. The solution was evaporated overnight

under vacuum to obtain a thin lipid film. Then 350 μL of buffer (Britton-Robinson buffer, pH 7.4) solution was added, and the resulting mixture stirred until formation of crude suspension. The suspension was subjected to 5 cycles of freezing in liquid nitrogen and thawing at 60 °C, followed by 21-fold extrusion with Avanti Mini-Extruder (Avanti Polar Lipids, Birmingham, AL, USA) through a 100-nm polycarbonate filter (Avanti 610005) at 50 °C. As a result, unilamellar vesicles with an average diameter of 110 nm were obtained. The concentrations of a lipid in stock suspension were 63 mM + 7 mM (DPPC + POPG).

Turbidimetry. Experiments to determine the temperature of the phase transition were carried out by measuring the turbidity of a dilute lipid suspension (0.7 mM) on a UV-3600 spectrophotometer (Shimadzu, Kyoto, Japan) equipped with Peltier temperature control unit, the thickness of the transmission layer was 1 cm, the slit width was 1 nm, and the wavelength was 400 nm. Titration of the lipid by the test compounds was carried out in quartz cells. To reduce the experimental error, the obtained compounds were added to 3 mL of a lipid suspension (0.7 mmol) as their concentrated solutions into a buffer (Britton-Robinson buffer, pH 7.4). To determine the temperature of the lipid phase transition, we measured the optical density of the samples in the temperature range 34.3–40.0 °C in steps of 0.1 °C per minute. Experimental data on the dependence of the optical density of the emulsion of the vesicles were mathematically processed in the software package Origin 8.1 (OriginLab Corporation, Northampton, MA, USA) by the Vant-Hoff 2-state model giving the phase transition temperature (Tm) of the system.[S2]

Transmission electron microscopy (TEM). TEM analysis of the samples was carried out using the JEOL JEM 100CX II transmission electron microscope. For sample preparation, 10 μL of the 1×10^{-5} M suspension were placed on the Formvar/carbon-coated 3 mm copper grid, which was then dried at room temperature. After complete drying, the grid was placed into the transmission electron microscope using special holder for microanalysis.

Molecular docking. The AutoDock Vina program [S3,S4] was used to estimate binding energies of the following complexes: ciprofloxacin-OqxB, ciprofloxacin-pillar[5]arene, pillar[5]arene-OqxB. Crystal structure of OqxB efflux pump (PDB ID: 7CZ9) was obtained from Protein Data Bank.[S5] Water and substrate molecules were removed from downloaded PDB file before docking simulations. The structures of the ciprofloxacin and pillar[5]arene molecules were optimized by XTB program package.[S6] In all docking simulations a receptor was rigid, while a ligand was flexible. To dock ciprofloxacin to pillar[5]arene, the several isomers of macromolecule were obtained by MD simulations with Gromacs software.[S7] Ligand-residue interactions were detected and visualized with Protein-Ligand Interaction Profile (PLIP) web tool. MD simulations were also performed to check stability of ciprofloxacin-pillar[5]arene complexes. The topology files of the molecules were obtained with Automated Topology Builder (ATB), [S8,9] based on GROMOS96 54a7 force field.[S10] The systems containing one pillar[5]arene and two ciprofloxacin molecules were solvated using the simple point charge (SPC) [S11] water model in an orthorhombic box. After energy minimization the position-restricted NVT and NPT equilibrations were performed on the system for 100 ps. Then 20 ns MD simulations were carried out under NPT conditions. A modified Berendsen (300K, $\tau T = 0.1$ ps) and Parrinello−Rahman barostat (1 atm., $\tau p = 2$ ps) were used during simulations. A time step 1 fs was used in the leapfrog algorithm [S12] and coordinates were stored every 5 ps. A single-range cutoff limit of 1.4 nm was set for

electrostatic and van der Waals interactions. The long-range electrostatic interactions were calculated using the Particle Mesh Ewald (PME) method.[S13] H-bonds were limited by LINCS algorithm.[S14]

2. Synthesis of the compounds 2 and 3

4,8,14,18,23,26,28,31,32,35- deca-[(tetraacetyl-(β-D-glycoside))thioethoxy]-pillar[5]arene (**2**)

Dry K_2CO_3 (0.29 g, 2.14 mmol) and 1-thio-β-D-glucose tetraacetate (0.39 g, 1.07 mmol) were placed into a round-bottom flask equipped with a magnetic stirrer, which was stirred under cooling in an ice bath with 8 mL of anhydrous DMF. Then decabromethoxypillar[5]arene 1 (0.1 g, 0.06 mmol) was added, the reaction was carried out for 56 hours at a temperature of 90 °C in an argon atmosphere. After the reaction mixture was poured into distilled water by precipitation. The resulting brown precipitate was filtered. The reaction mixture was recrystallized from the CH_2Cl_2:H_2O solvent system, washed with water (3×30 mL), and evaporated on a rotary evaporator.

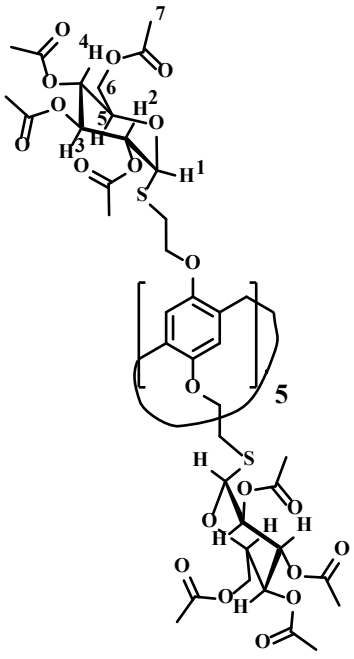

Yield: 0.24 g (88%).

^{1}H NMR ($CDCl_3$): 0.97 – 2.04 m (120H, H^7), 3.05 – 3.12 m (20H, -CH_2S-), 3.43 – 4.09 m (30H, -CH_2-, -OCH_2-), 4.12 – 4.25 m (30H, H^5, H^6), 4.66 – 4.74 m (10H, H^2), 5.05 – 5.14 m (20H, H^1, H^4), 5.24 – 5.32 m (10H, H^3), 6.83 s (10H, ArH).

^{13}C{^{1}H} NMR ($CDCl_3$): 20.74, 30.06, 31.76, 62.17, 68.39, 69.92, 73.88, 75.91, 83.18, 115.75, 129.08, 149.73, 163.14, 169.57, 170.24, 170.70, 170.73.

IR (ν, cm^{-1}): 2942(-C_{Ar}-H), 2871(-C-H), 1741(-C=O), 1576(-C_{Ar}-C_{Ar}-), 1497(-CH_2-), 1436(-CH_3), 1367(-CH_3), 1206(C_{Ar}-O-CH_2), 1090(-C_{Ar}-H), 1030(-C_{Ar}-O-CH_2-).

MS (MALDI-TOF): calc. $[M]^+$ m/z = 4513.205, Found $[M+K]^+$ m/z = 4552.297

Found (%): C, 51.93; H, 5.54; S, 7.11. Calc. for $C_{195}H_{250}O_{100}S_{10}$ (%): C, 51.88; H, 5.58; S, 7.10

4,8,14,18,23,26,28,31,32,35-deca-[(β-D-glycoside))thioethoxy]-pillar[5]arene (**3**)

Macrocycle **2** (0.24 g, 0.05 mmol) and CH_3ONa (0.1 g, 1.85 mmol) was solved in 10 mL CH_3OH in a round-bottomed flask equipped with a magnetic stirrer. The reaction was carried out for 2 hours at room temperature The resulting brown precipitate was filtered, washed with CH_3OH (3×10 mL), dissolved in water and evaporated on a rotary evaporator.

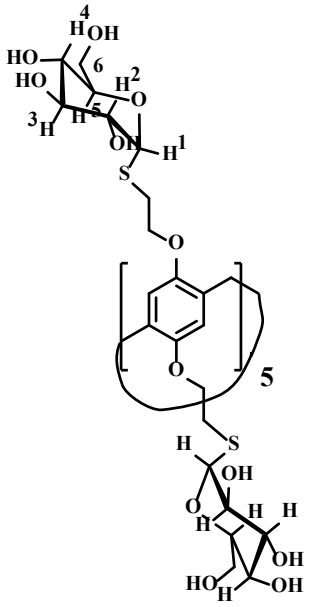

Yield: 0.14 g (92%).

^{1}H NMR (DMSO-*d*$_6$): 3.04 – 3.19 m (50H, -CH$_2$S-, H^5, H^6), 3.44 – 3.47 m (20H, H^3, H^4), 3.48 – 3.66 m (10H, -CH$_2$-), 3.66 – 3.69 m (10H, H^2), 3.97, 4.31m (20H, -OCH$_2$-), 4.39 – 4.48 m (10H, H^1), 6.91 s (10H, H$_{Ar}$).

^{13}C{^{1}H} NMR (DMSO-*d*$_6$): 29.13, 30.69, 61.17, 68.15, 69.92, 73.30, 78.13, 80.88, 84.99, 85.45, 114.91, 128.44, 149.03.

IR (ν, cm^{-1}): 3304(-OH), 2867 (C$_{Ar}$-H), 1576(-C$_{Ar}$-C$_{Ar}$-), 1496(-CH$_2$-), 1404(-OH), 1376(-CH$_2$-), 1278(O-CH$_2$), 1204(C$_{Ar}$-O-CH$_2$), 1098(-C$_{Ar}$-H), 1020(-C$_{Ar}$-O-CH$_2$-).

MS (ESI): calc. [M]$^+$ m/z = 2925.042, Found [M+K$^+$+Li$^+$]$^{2+}$ m/z = 1439.3397.

Found (%): C, 48.80; H, 5.99; S, 11.30. Calc. for C$_{115}$H$_{170}$O$_{60}$S$_{10}$ (%): C, 48.75; H, 6.05; S, 11.32.

3. NMR, MALDI TOF MS, IR spectra of the compounds 2, 3

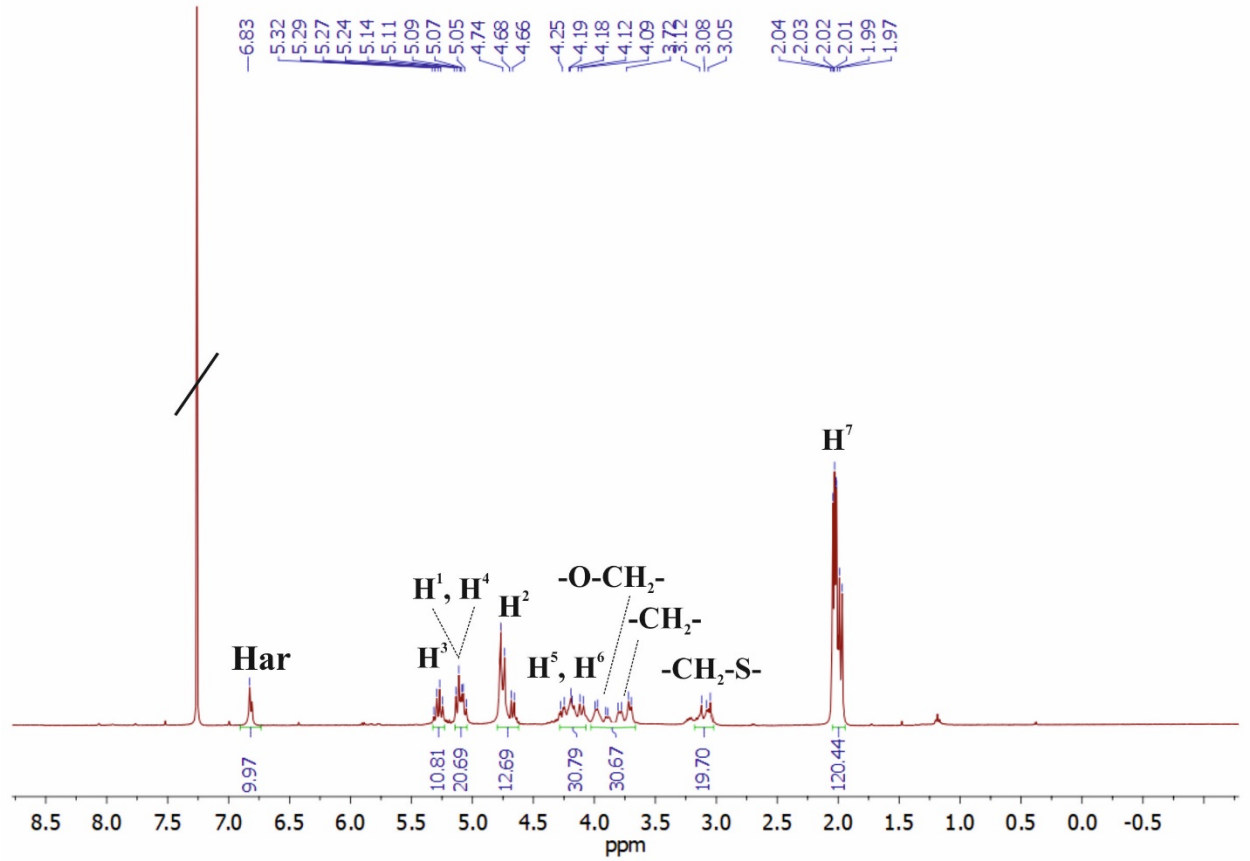

Figure S1. ^{1}H NMR spectrum of **4,8,14,18,23,26,28,31,32,35-deca-[(tetraacetyl-(β-D-glycoside))thioethoxy]-pillar[5]arene** (**2**). CDCl$_3$, 298 K, 400 MHz.

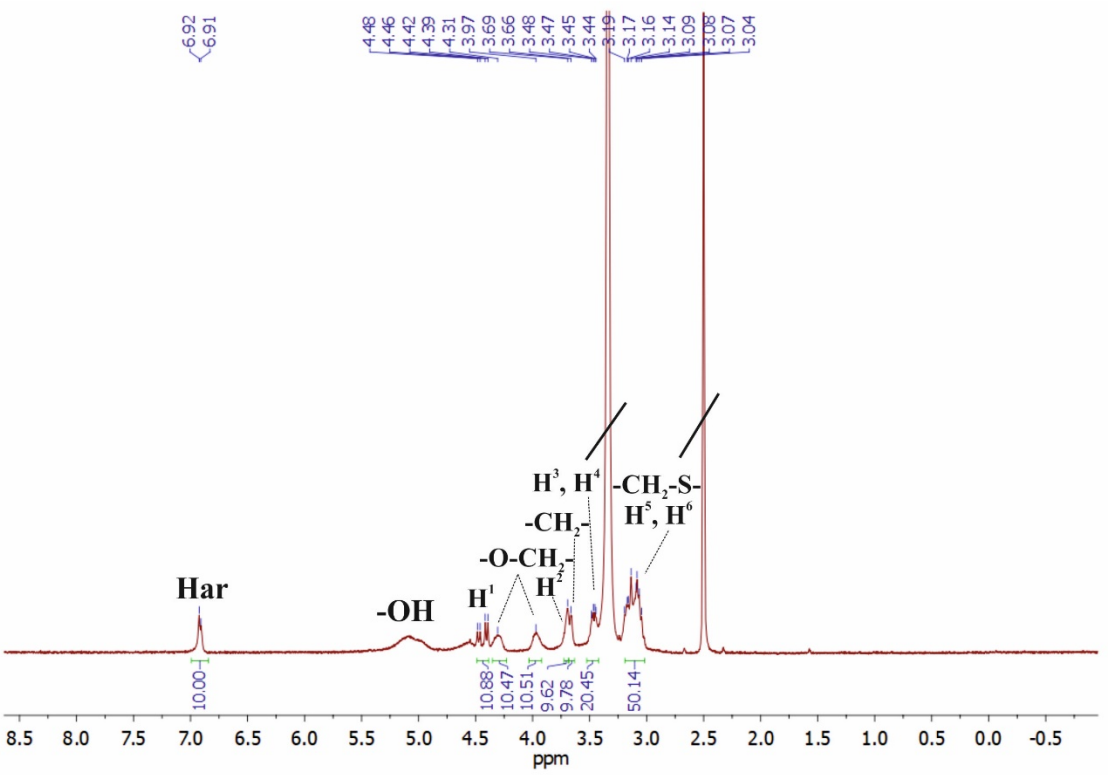

Figure S2. ^{1}H NMR spectrum of **4,8,14,18,23,26,28,31,32,35-deca-[(β-D-glycoside)thioethoxy]-pillar[5]arene** (**3**). DMSO-*d*$_6$, 298 K, 400 MHz.

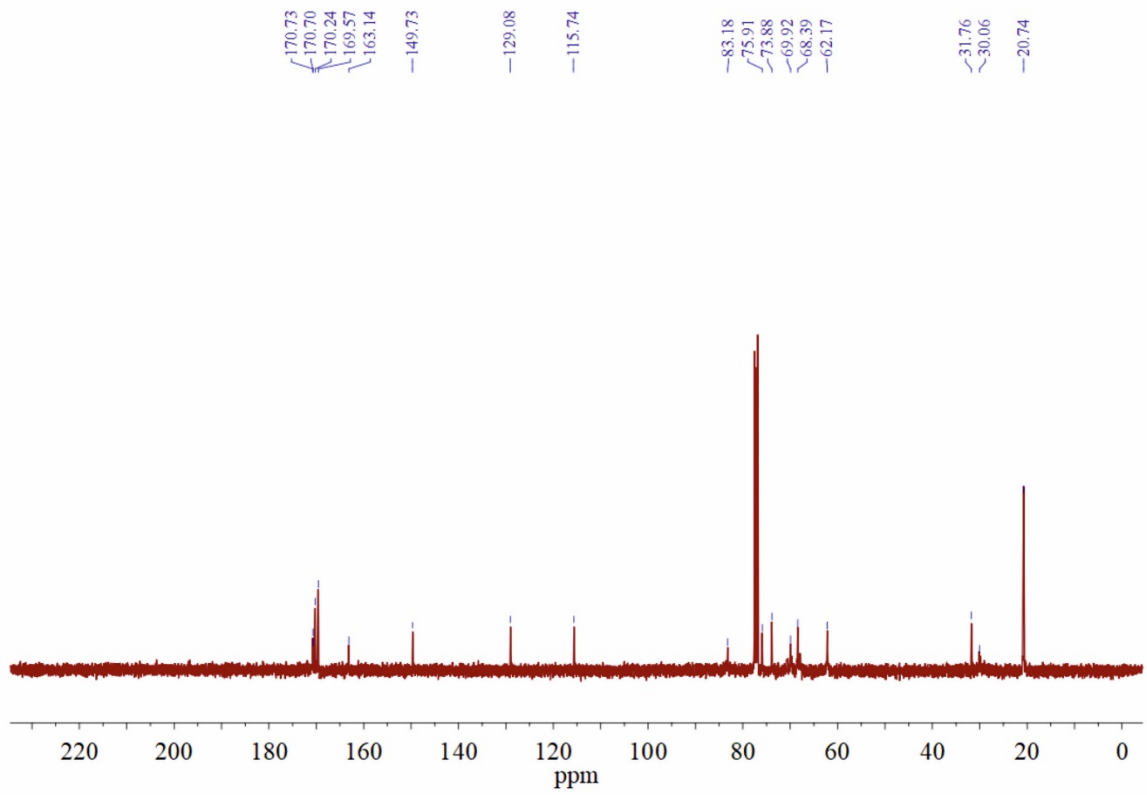

Figure S3. ^{13}C NMR spectrum of **4,8,14,18,23,26,28,31,32,35-deca-[(tetraacetyl-(β-D-glycoside))thioethoxy]-pillar[5]arene** (**2**). $CDCl_3$, 298 K, 400 MHz.

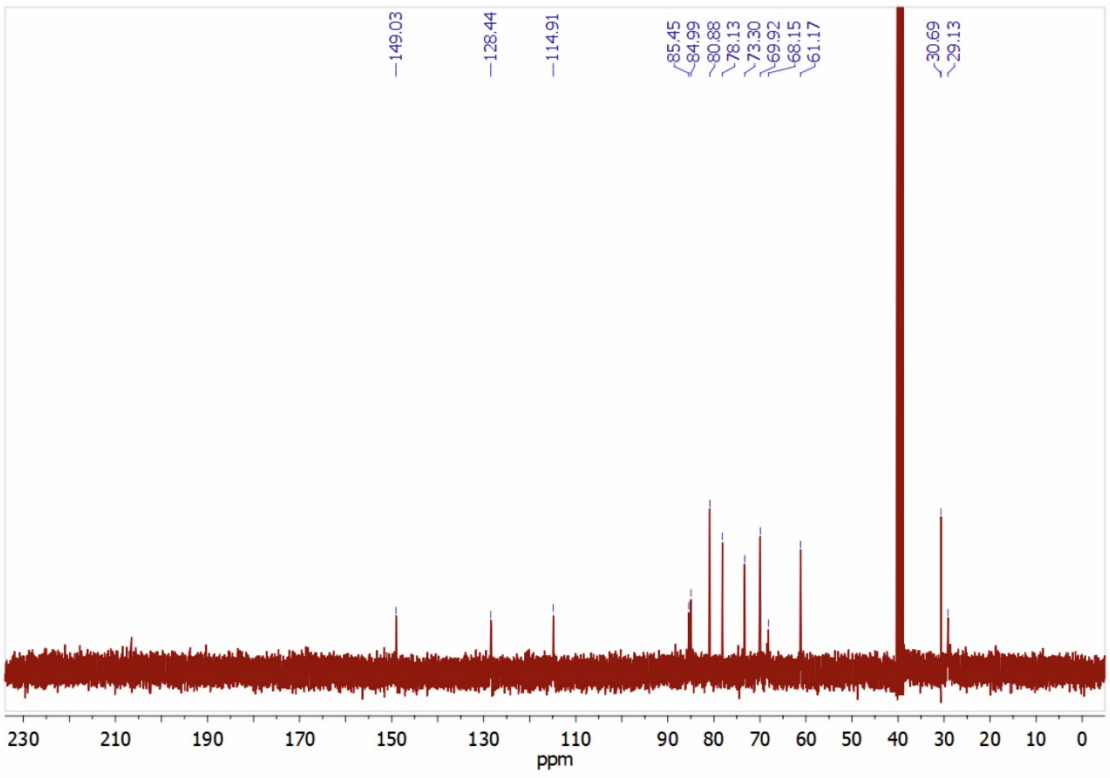

Figure S4. ^{13}C NMR spectrum of **4,8,14,18,23,26,28,31,32,35-deca-[(β-D-glycoside))thioethoxy]-pillar[5]arene** (**3**). DMSO-*d*$_6$, 298 K, 400 MHz.

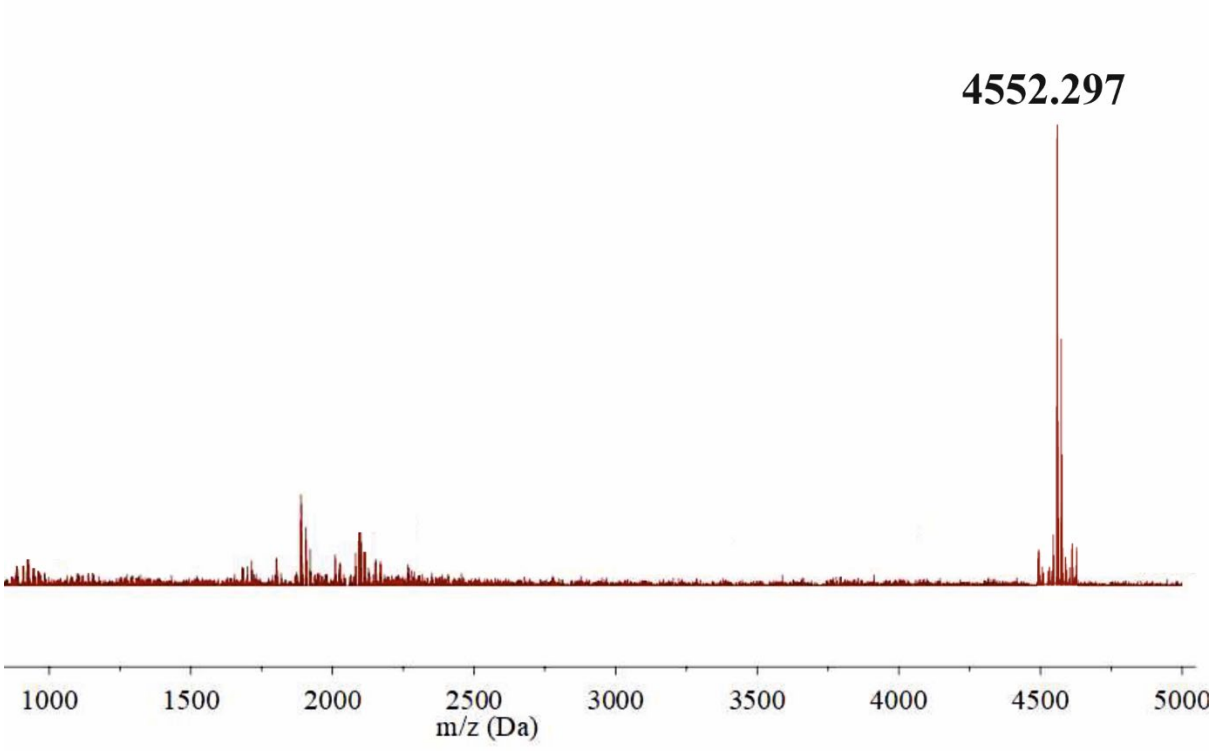

Figure S5. Mass spectrum (MALDI-TOF, 4-nitroaniline matrix) of **4,8,14,18,23,26,28,31,32,35- deca-[(tetraacetyl-(β-D- glycoside))thioethoxy]-pillar[5]arene** (**2**).

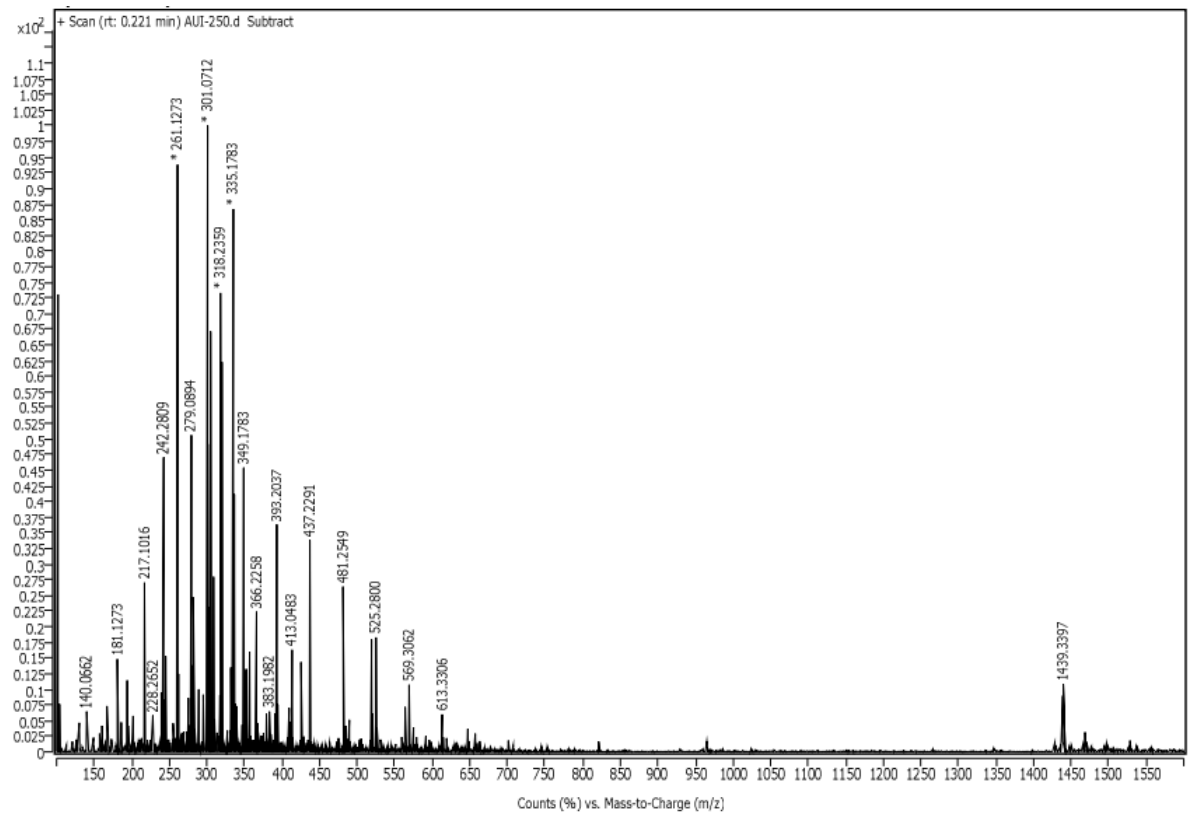

Figure S6. Mass spectrum (ESI) of **4,8,14,18,23,26,28,31,32,35-deca-[(β-D-glycoside))thioethoxy]-pillar[5]arene** (**3**).

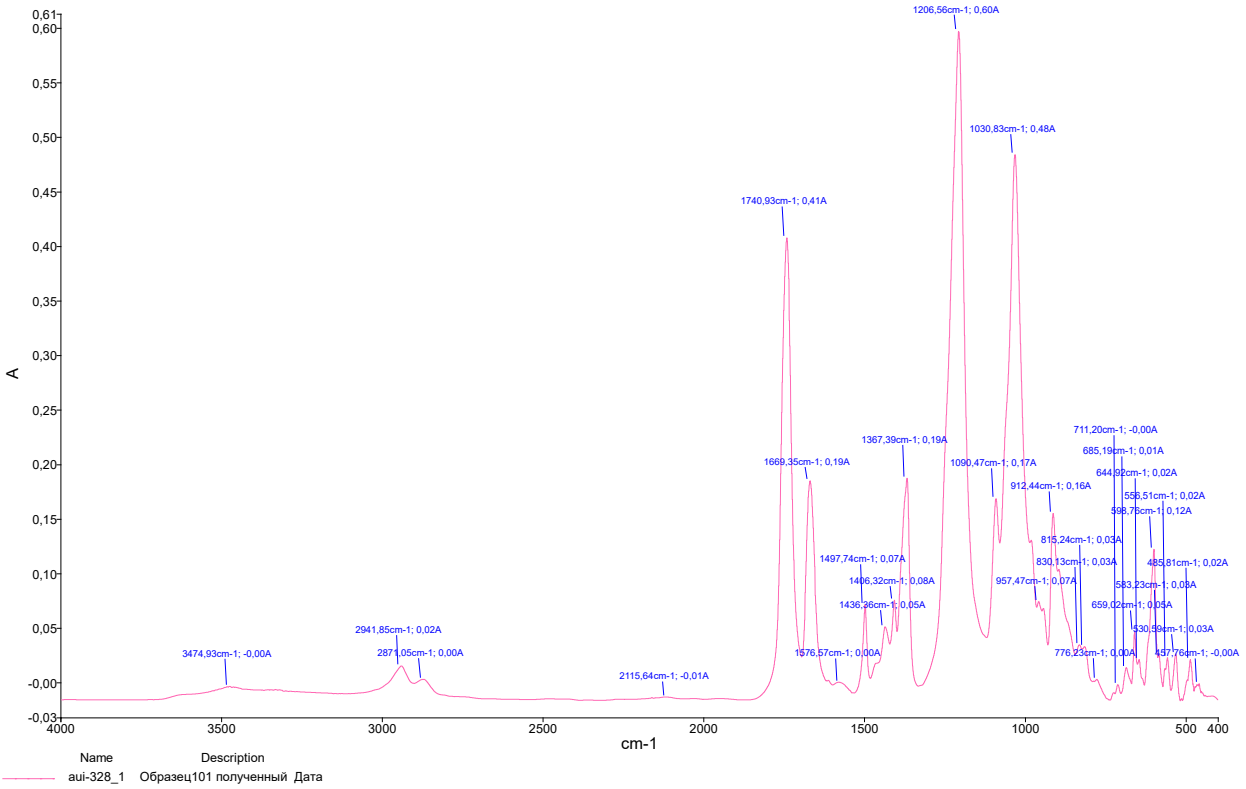

Figure S7. IR spectrum of **4,8,14,18,23,26,28,31,32,35- deca-[(tetraacetyl-(β-D-glycoside))thioethoxy]-pillar[5]arene** (**2**).

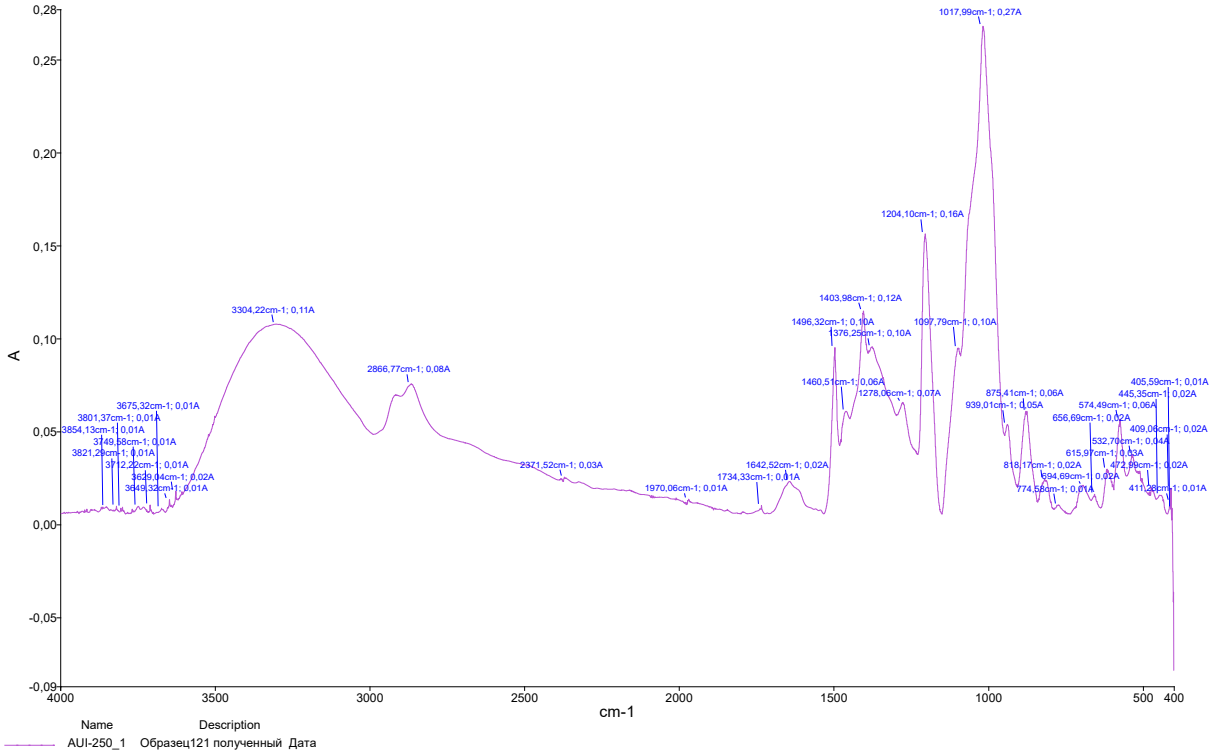

Figure S8. IR spectrum of **4,8,14,18,23,26,28,31,32,35-deca-[(β-D-glycoside))thioethoxy]-pillar[5]arene** (**3**).

4. UV-*vis* study

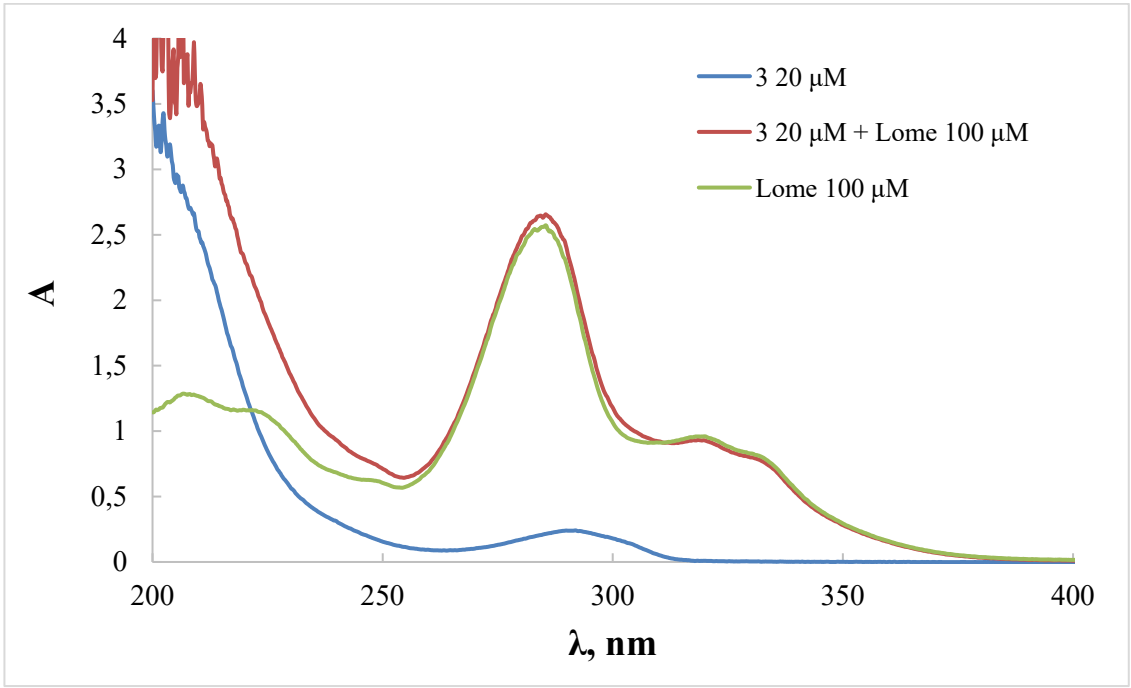

Figure S9. UV-*vis* spectra of macrocycle **3** (2×10^{-5} M), Lome (1×10^{-4} M) and mixture of **3** (2×10^{-5} M) / Lome (1×10^{-4} M) in water.

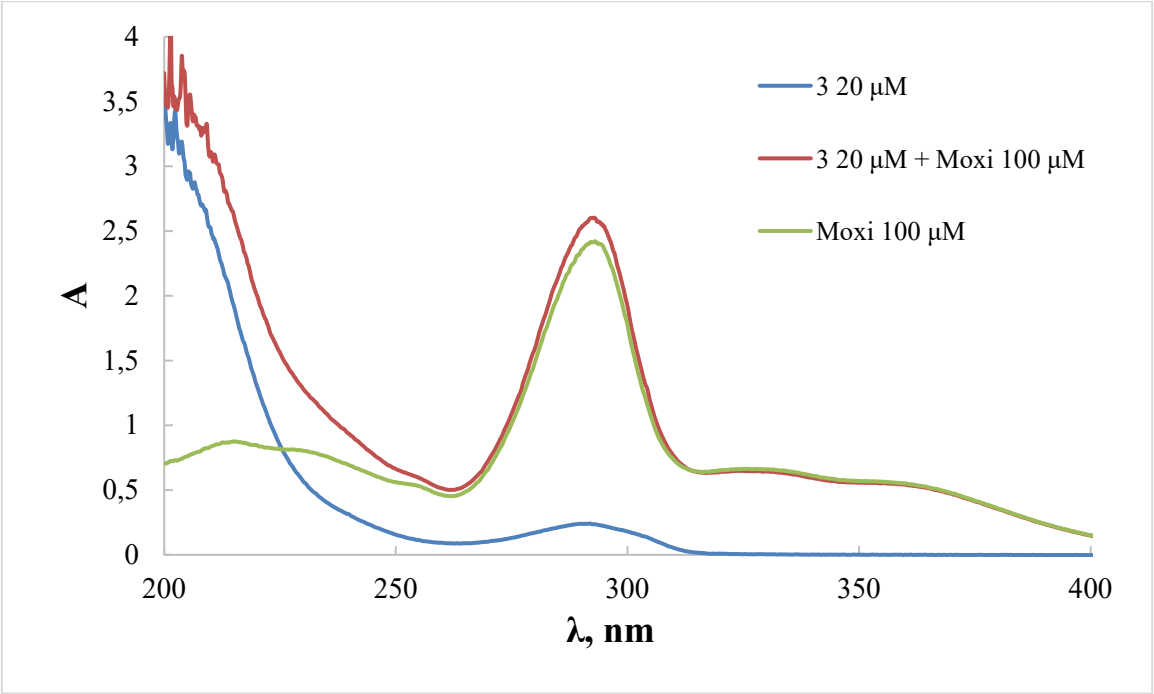

Figure S10. UV-*vis* spectra of macrocycle **3** (2×10^{-5} M), Moxi (1×10^{-4} M) and mixture of **3** (2×10^{-5} M) / Moxi (1×10^{-4} M) in water.

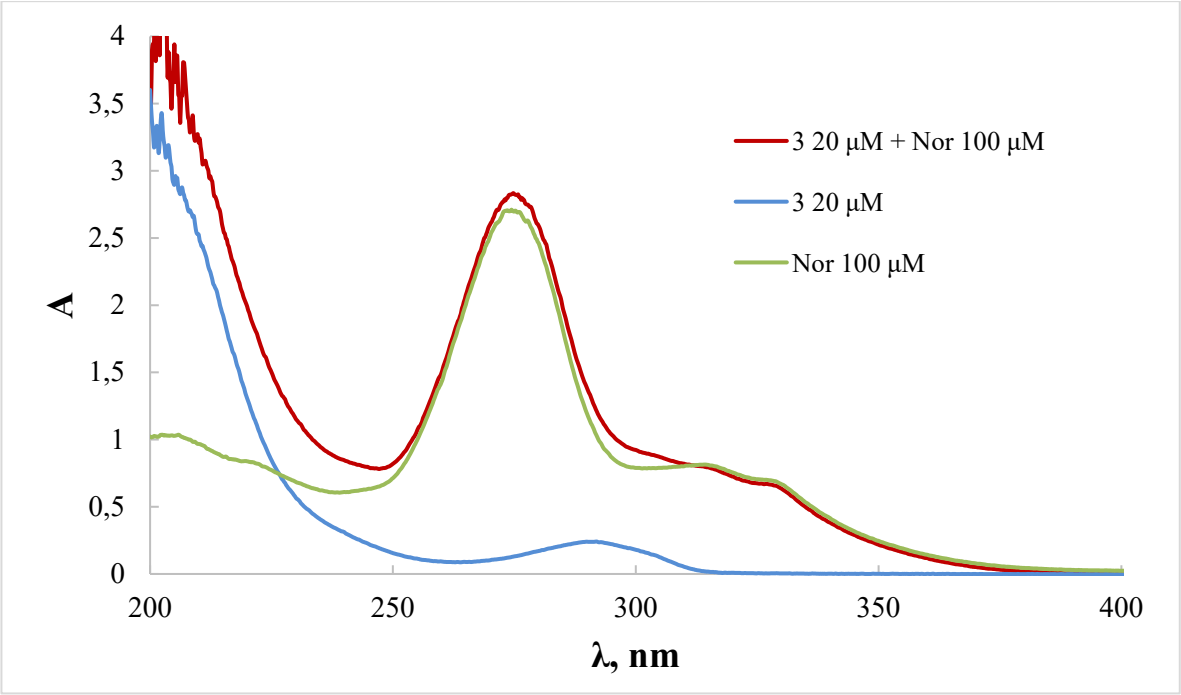

Figure S11. UV-*vis* spectra of macrocycle **3** (2×10^{-5} M), Nor (1×10^{-4} M) and mixture of **3** (2×10^{-5} M) / Nor (1×10^{-4} M) in water.

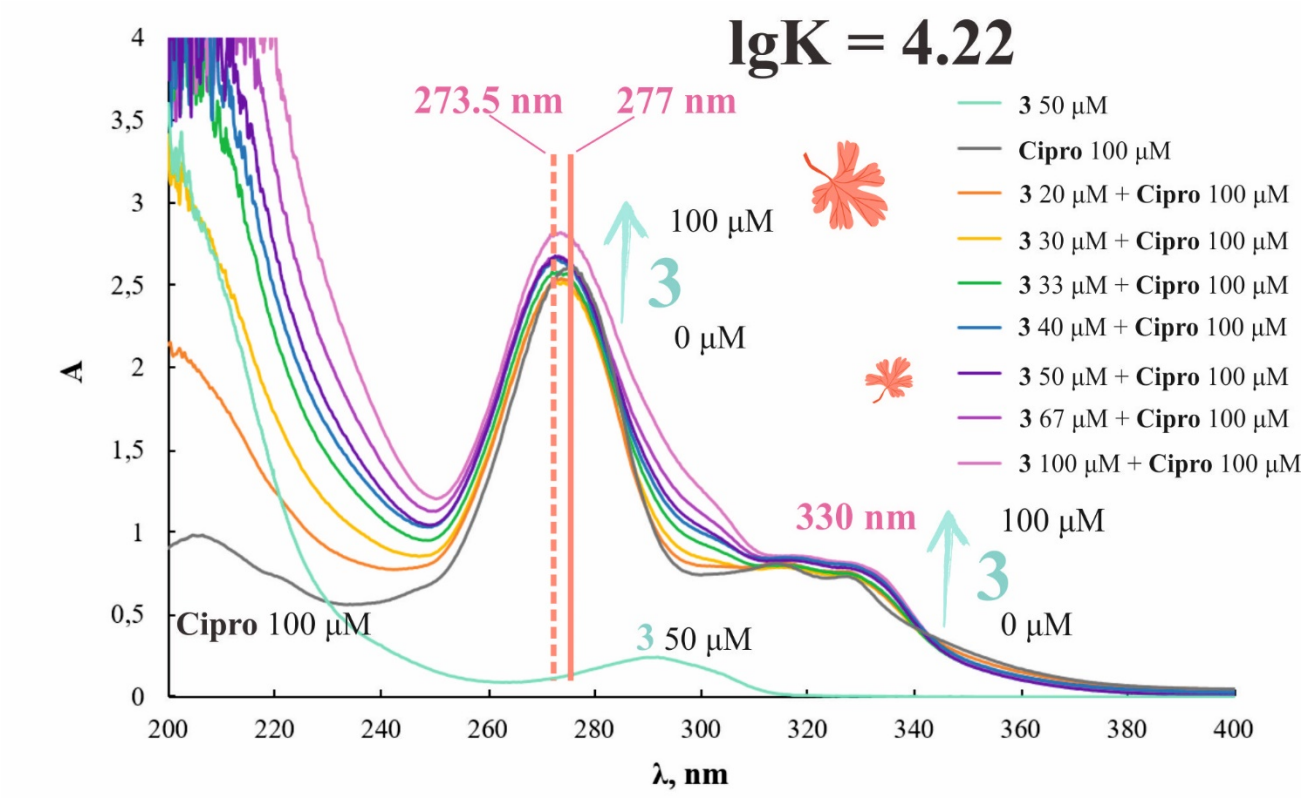

Figure S12. UV-*vis* spectra for Cipro (1×10^{-4} M) with **3** (1×10^{-5}-1×10^{-4} M) in water.

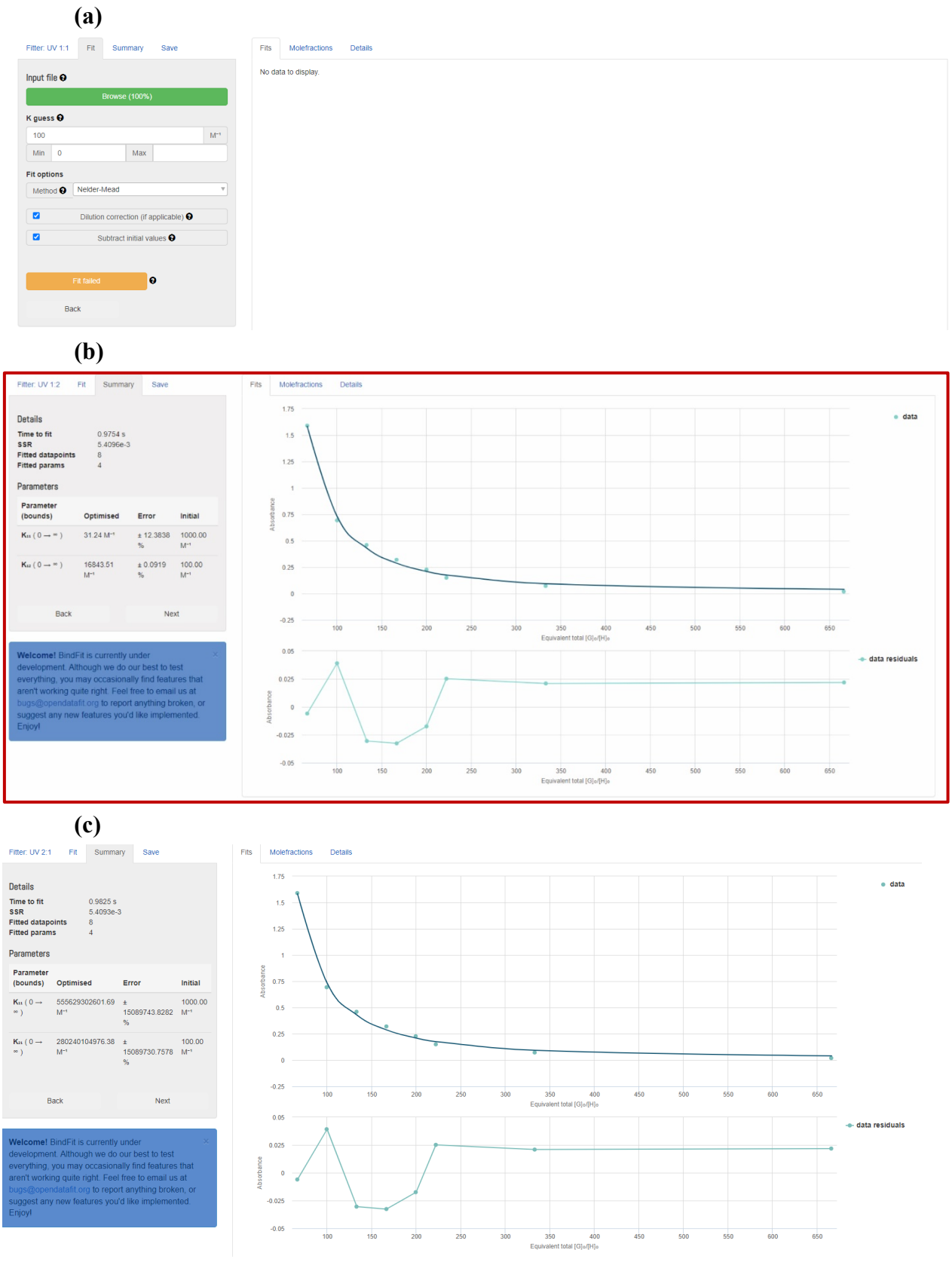

Figure S13. Bindfit (Fit data to 1:1, 1:2 and 2:1 Host-Guest equilibria) Screenshots taken from the summary window of the website supramolecular.org. This screenshots shows the raw data for UV-vis titration of **3** with Cipro, the data fitted to 1:1 binding model (a), 1:2 binding model (b) and 2:1 binding model (c).

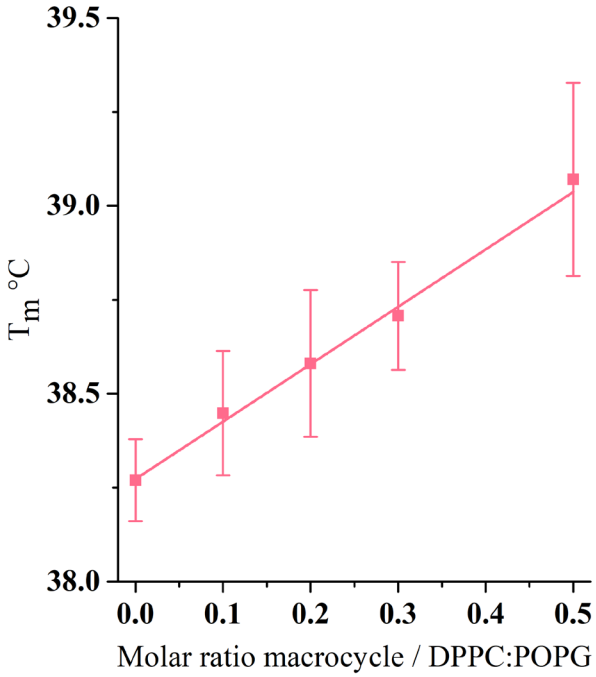

Molar ratio	T_m	T_mError±
0*	38.2701	0.1089
0.1	38.4482	0.1655
0.2	38.5804	0.1951
0.3	38.7072	0.1436
0.5	39.0703	0.2568

* Point 0 corresponds to Tm for lipids (DPPC:POPG) in the absence of compounds

y = 1.528x + 38.2727 (mathematical approximation of experimental data)

y – **T_m** (obtained experimentally using turbidimetry)

x – **Molar ratio**

$R^2 = 0.9927$

Figure S14. Linear dependence of Tm against molar ratio for compound **3**

5. Fluorescence study

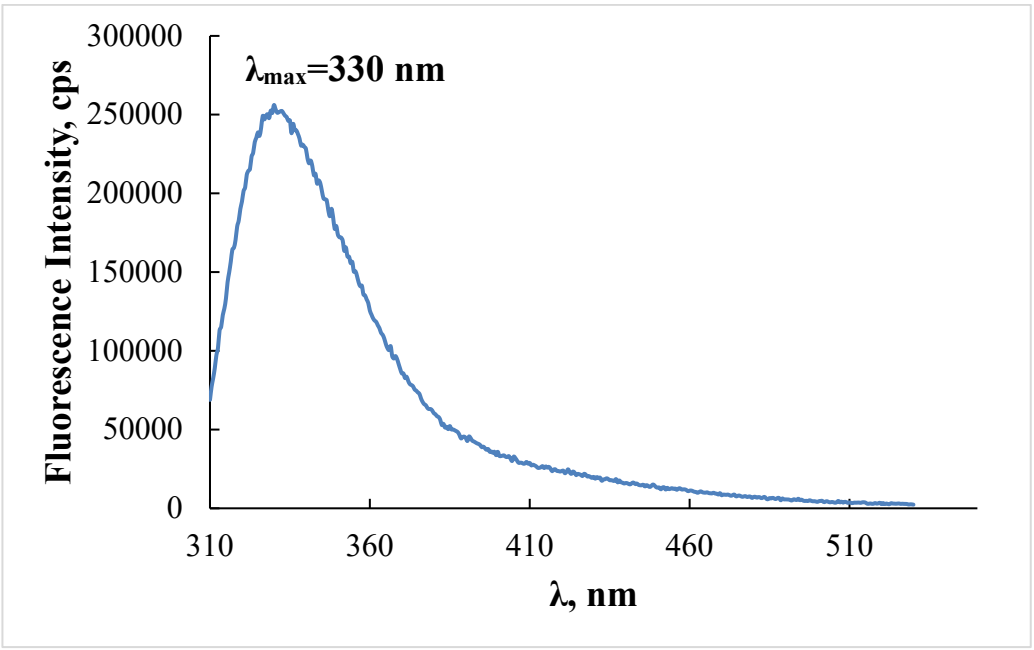

Figure S15. Fluorescence spectrum of **3** (2.5×10^{-5} M) in water (λ_{ex}= 280 нм).

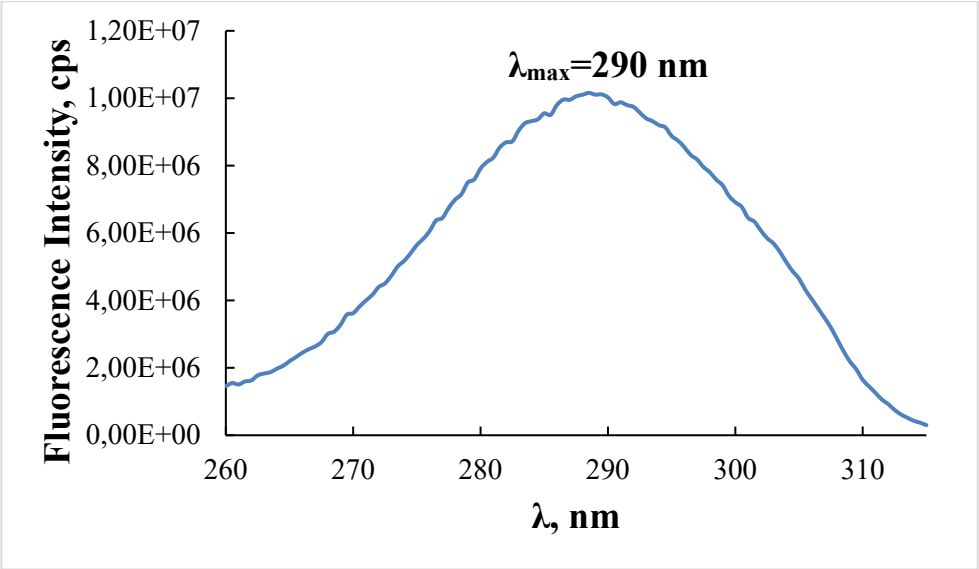

Figure S16. Excitation spectrum of **3** (2.5×10^{-5} M) in water (λ_{em}=330 nm).

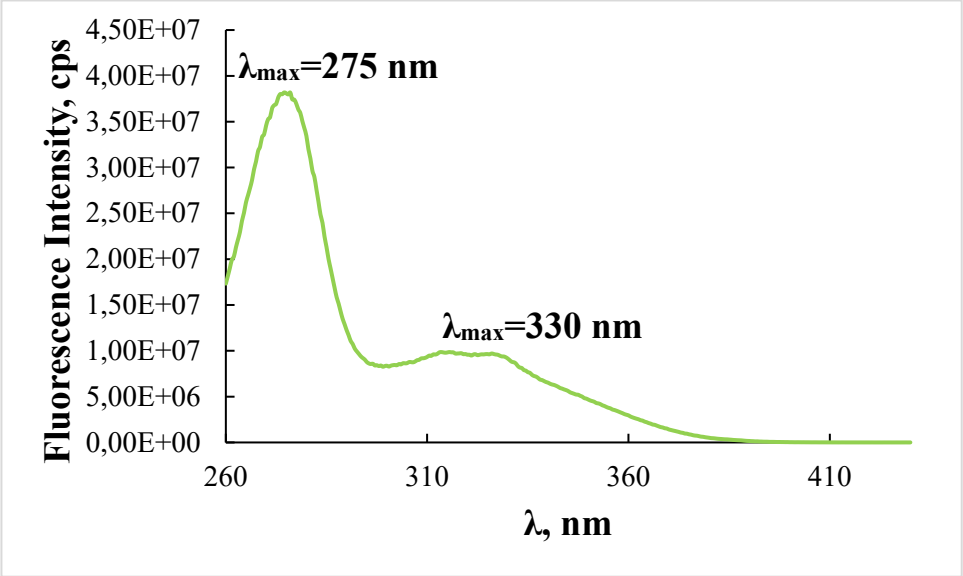

Figure S17. Excitation spectrum of **Cipro** (5×10^{-6} M) in water (λ_{em}=445 nm).

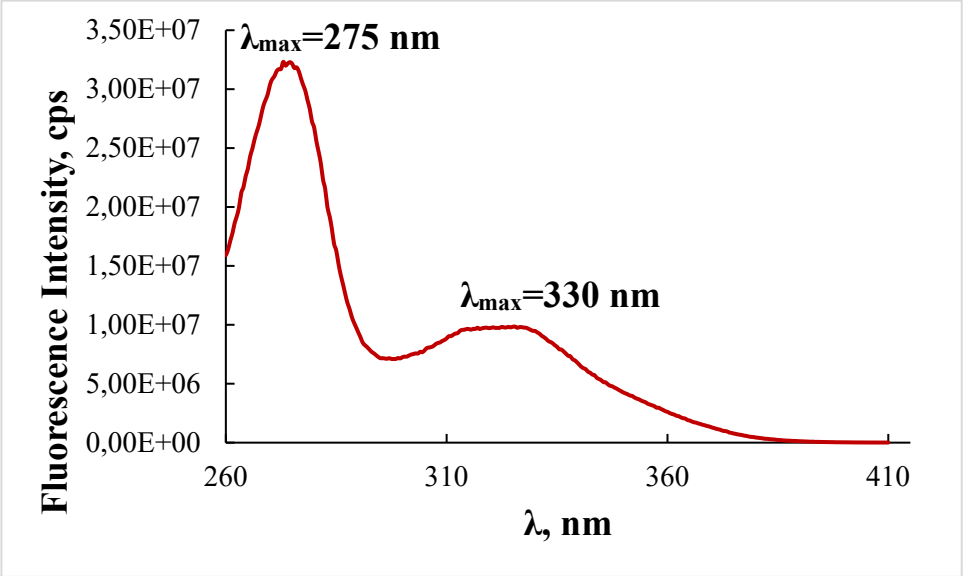

Figure S18. Excitation spectrum of Cipro (5×10^{-6} M) with **3** (3.5×10^{-5} M) in water (λ_{em}=425 nm).

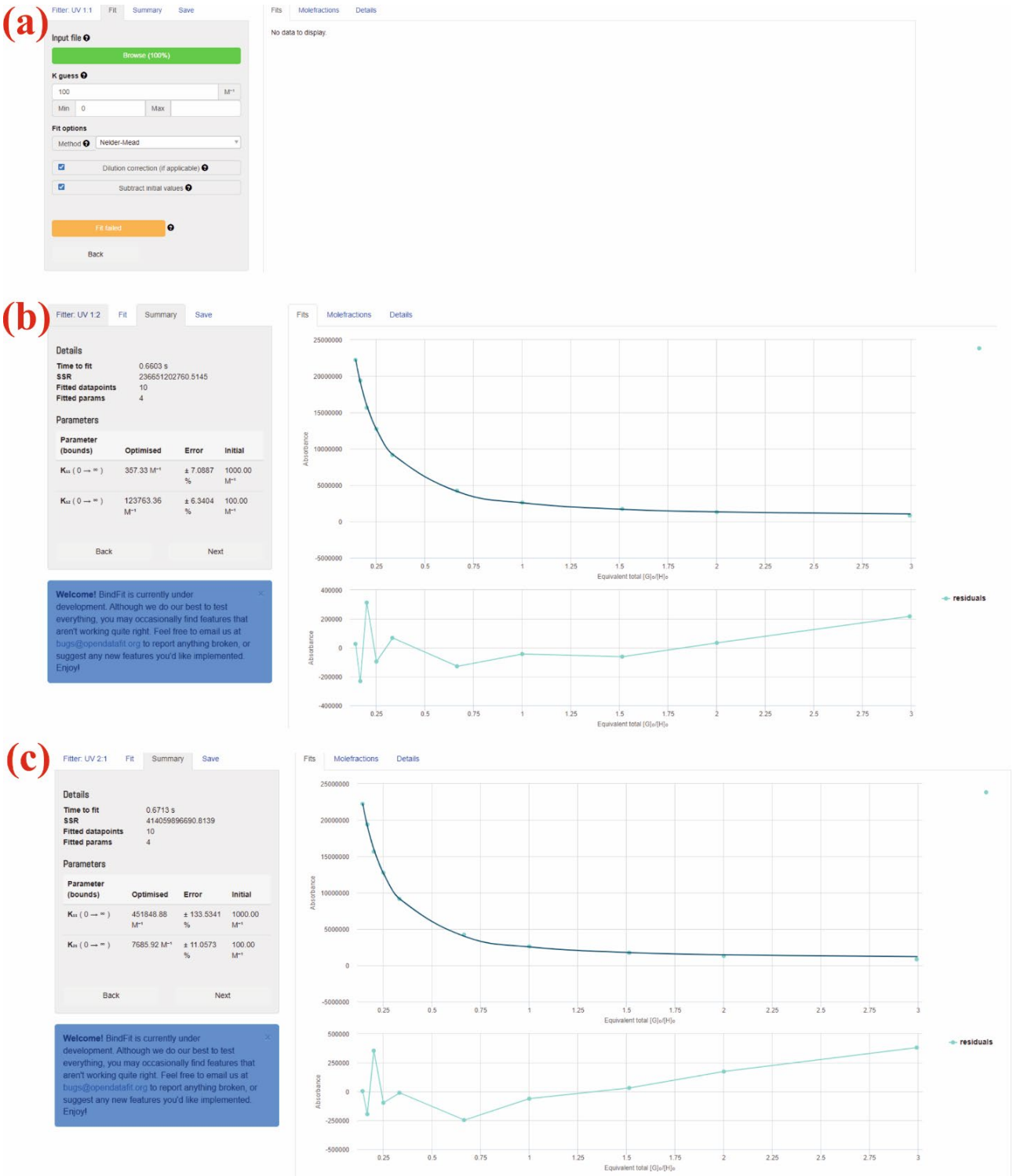

Figure S19. Bindfit (Fit data to 1:1, 1:2 and 2:1 Host-Guest equilibria) Screenshots taken from the summary window of the website supramolecular.org. This screenshots shows the raw data for Fluorescence titration of **3** with Cipro, the data fitted to 1:1 binding model (a), 1:2 binding model (b) and 2:1 binding model (c).

6. Critical aggregation concentration

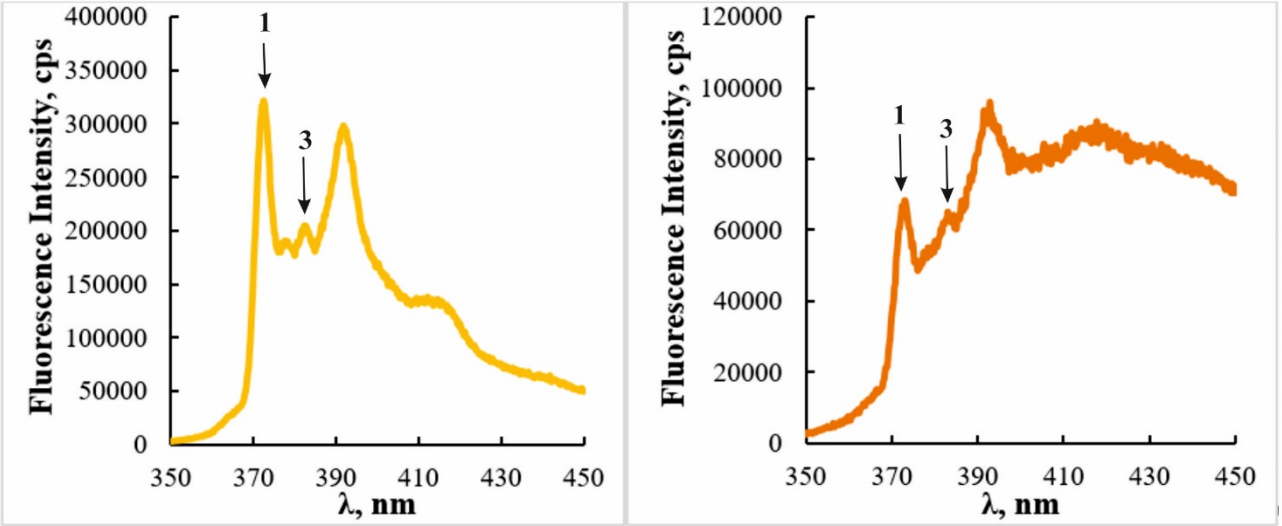

Figure S20. Fluorescence spectra of pyrene (1 μM) without/with **3** (750 μM) in water.

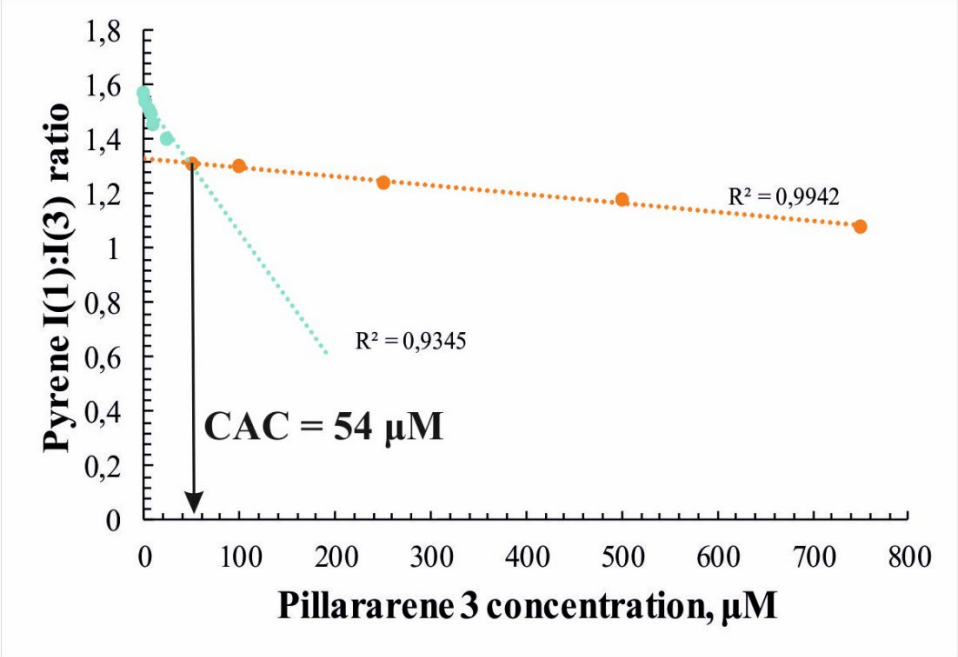

Figure S21. The ratio of the first and third pyrene emission peaks' (372 and 382 nm, respectively) intensities versus the concentration of **3** in water.

7. NMR study

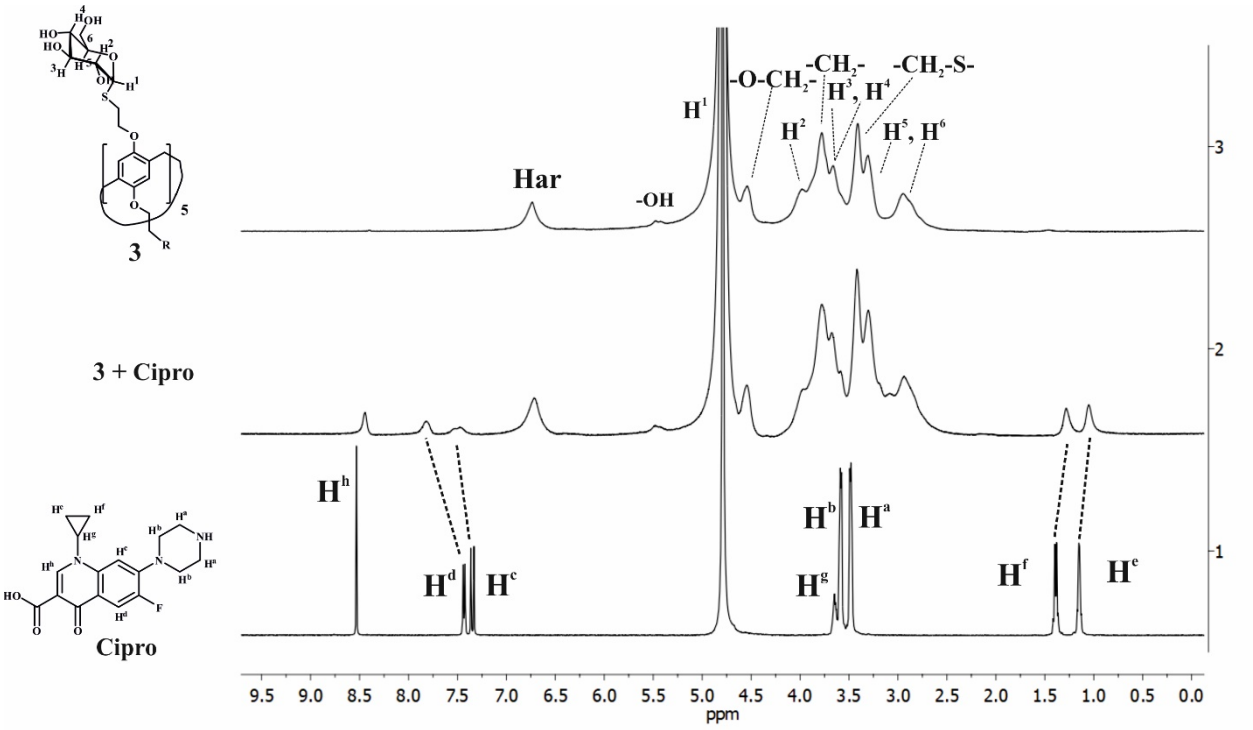

Figure S22. The ^{1}H NMR spectrum of: 1. Cipro (2×10^{-2} M); 2. **3** (1×10^{-2} M); 3. complex of **3** (1×10^{-2} M) / Cipro (2×10^{-2} M) in D_2O at 25 °C.

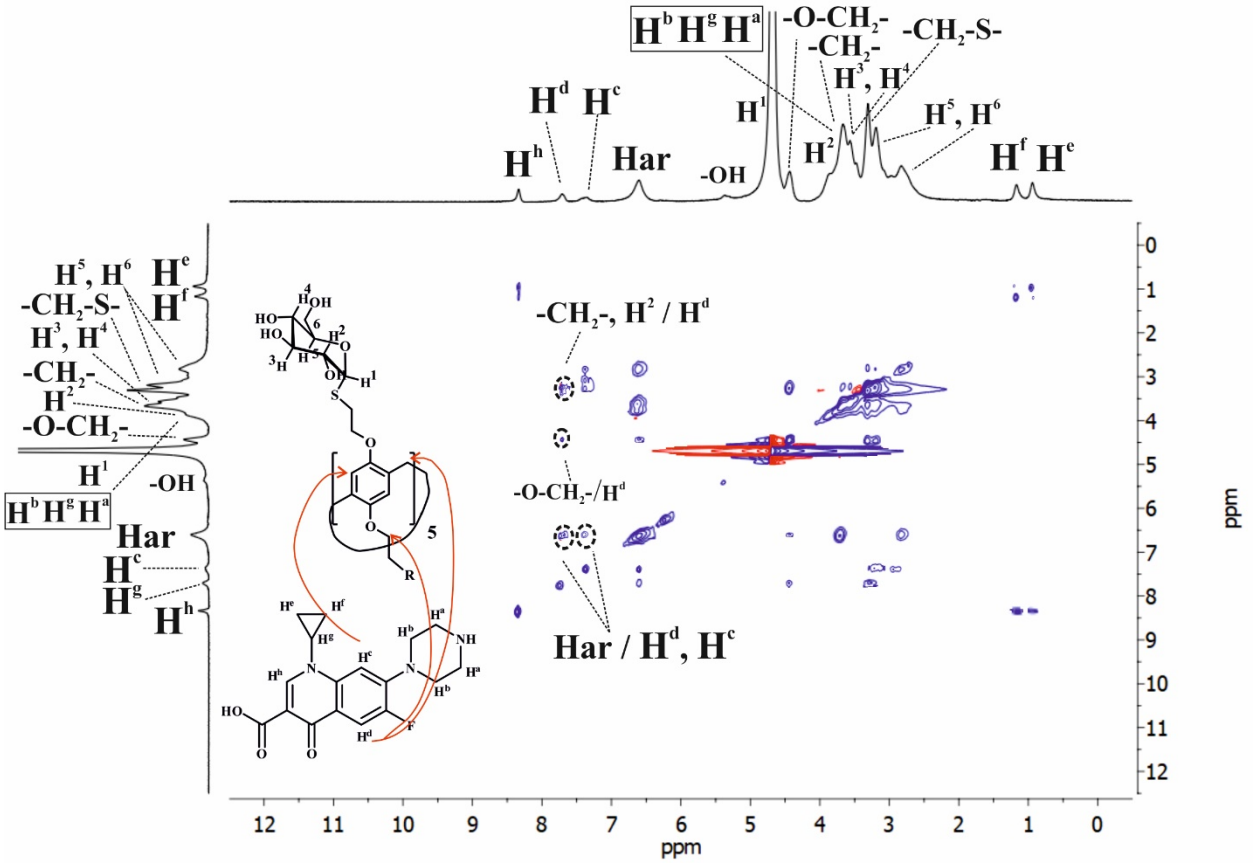

Figure S23. The 2D ^{1}H-^{1}H NOESY NMR spectrum of the complex **3** (1×10^{-2} M) / Cipro (2×10^{-2} M) in D_2O at 25 °C and the proposed structure of the complex.

8. Dynamic light scattering

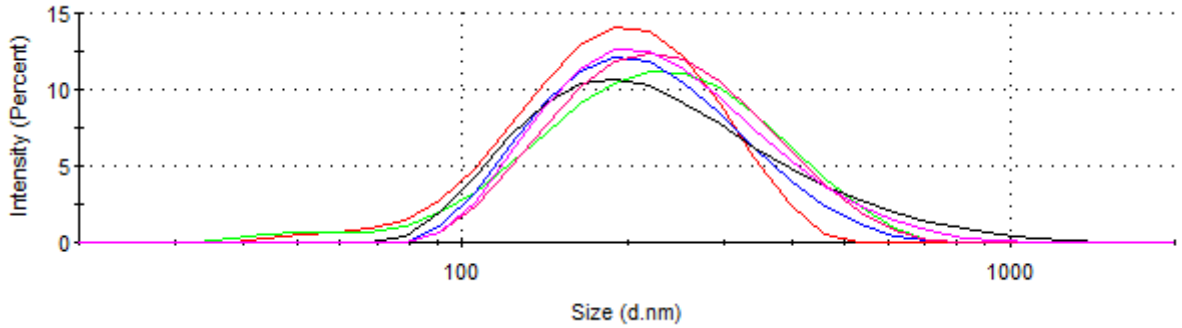

Figure S24. Size distribution of the particles by intensity for **3** (1×10^{-5} M) in water (d=228 ± 18 nm, PDI= 0.36 ± 0.05).

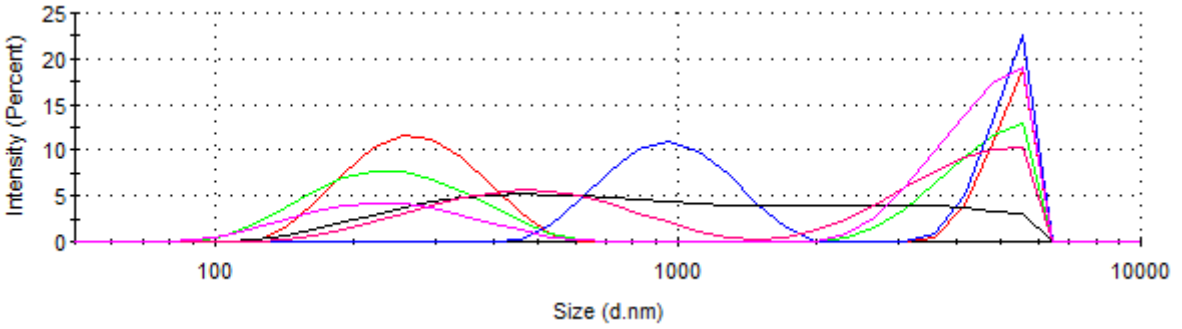

Figure S25. Size distribution of the particles by intensity for Cipro (1×10^{-4} M) in water (d=1597 ± 1085 nm, PDI= 0.74 ± 0.18).

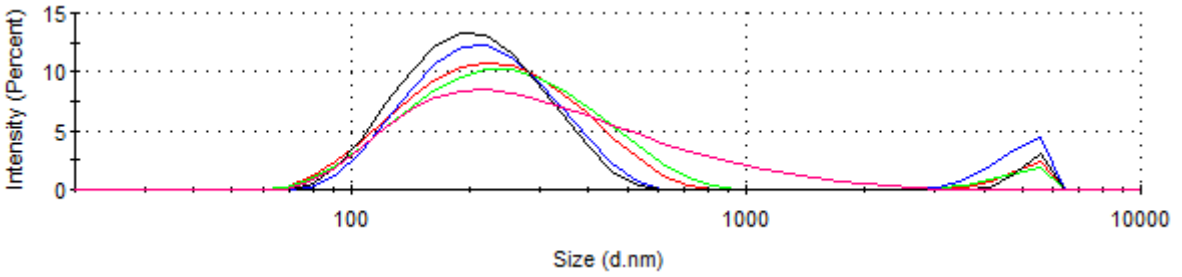

Figure S26. Size distribution of the particles by intensity for **3** (1×10^{-6} M) + Cipro (1×10^{-5} M) in water (d=283±15 nm, PDI= 0.30±0.05).

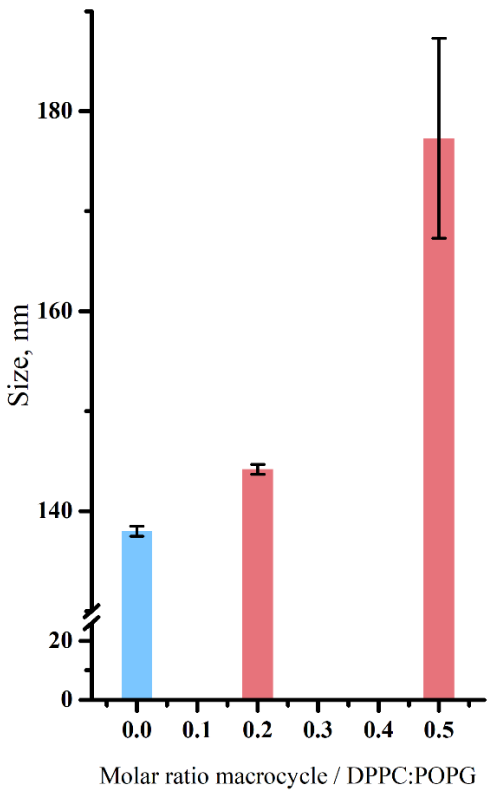

Molar ratio	Size, nm	PDI
0*	138.0±0.5	0.10
0.2	144.2±0.5	0.15
0.5	177.3±9.9	0.33

* Point 0 corresponds to size for lipids vesicles (DPPC:POPG) in the absence of compounds

Figure S27. Sizes of the vesicles DPPC:POPG (9:1) in the presence and absence of macrocycle **3.**

Table S1. Aggregation 3 with ciprofloxacin hydrochloride in water by DLS method

Sample	C_3, M	C_{Cipro}, M	$Z_{average}$ (d), nm	PDI	ζ-potential, mV
3	1×10^{-5}	0	229±18	0.36±0.05	5.2±1.8
Cipro	0	1×10^{-3}	606±243	0.61±0.16	-
Cipro	0	1×10^{-4}	1597±1085	0.74±0.18	-
Cipro	0	1×10^{-5}	-	-	-
3:Cipro	1×10^{-5}	1×10^{-4}	246±6	0.27±0.05	-15.6±1.1
3:Cipro	1×10^{-6}	1×10^{-5}	283±15	0.30±0.05	-17.2±0.3
3:Cipro	1×10^{-6}	2×10^{-6}	261±30	0.34±0.07	-
3:Cipro	1×10^{-6}	5×10^{-6}	292±53	0.41±0.21	-
3:Cipro	1×10^{-5}	5×10^{-7}	254±39	0.45±0.08	-

9. Morphology of 3, 3/Cipro

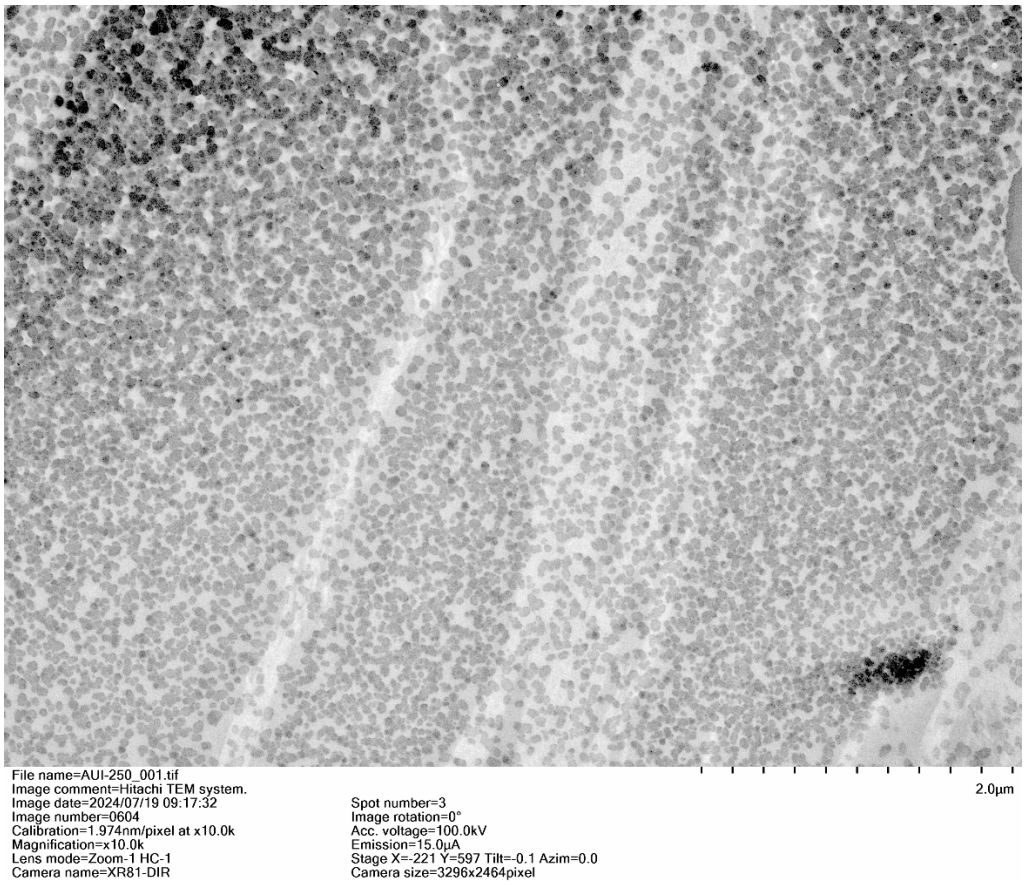

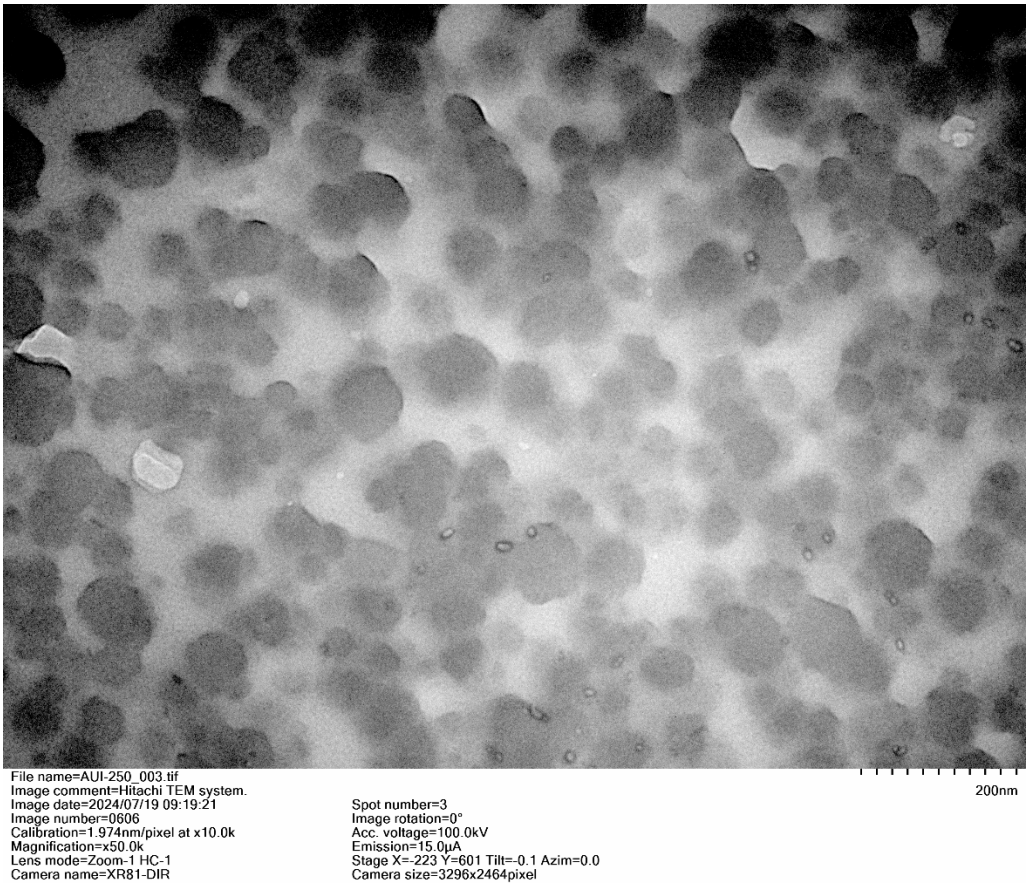

Figure S28. TEM images of **3** (1×10^{-5} M) after the solvent evaporation.

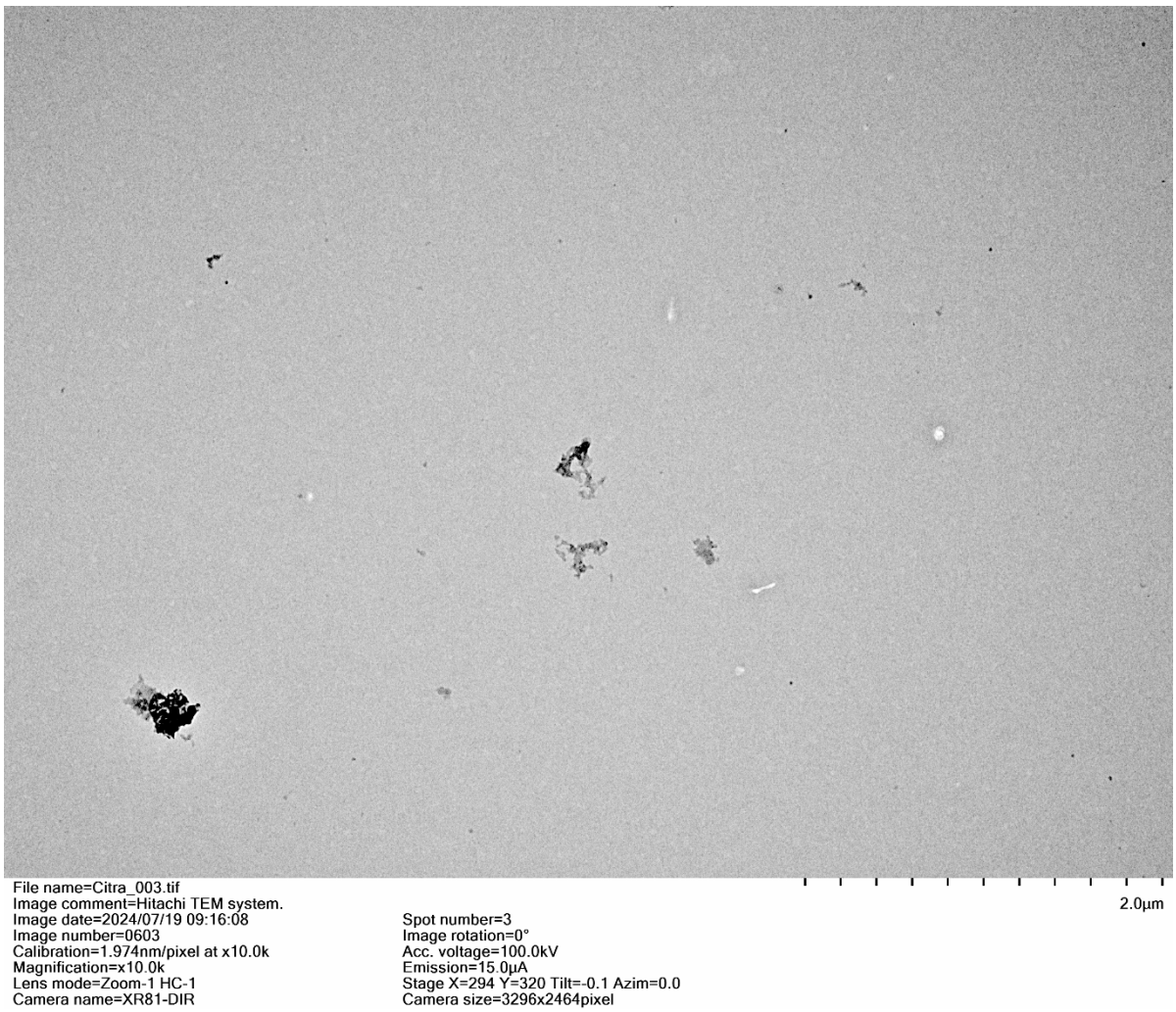

Figure S29. TEM image of Cipro (2×10^{-5} M) after the solvent evaporation.

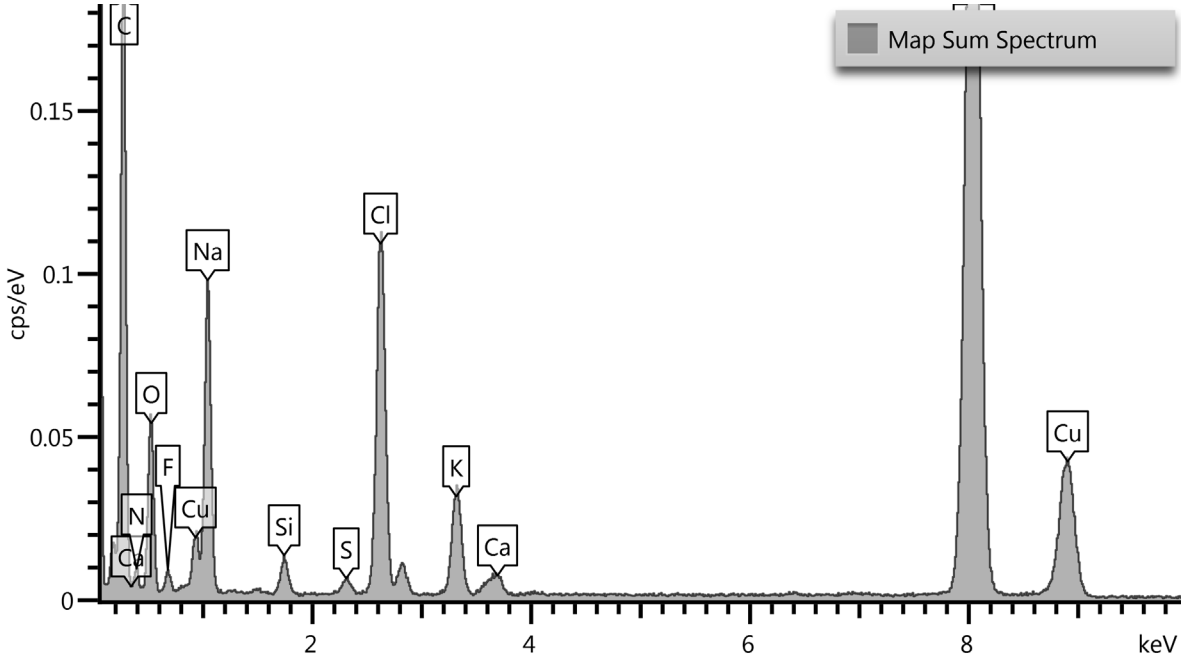

Figure S30. TEM-EDS spectra of **3** / Cipro

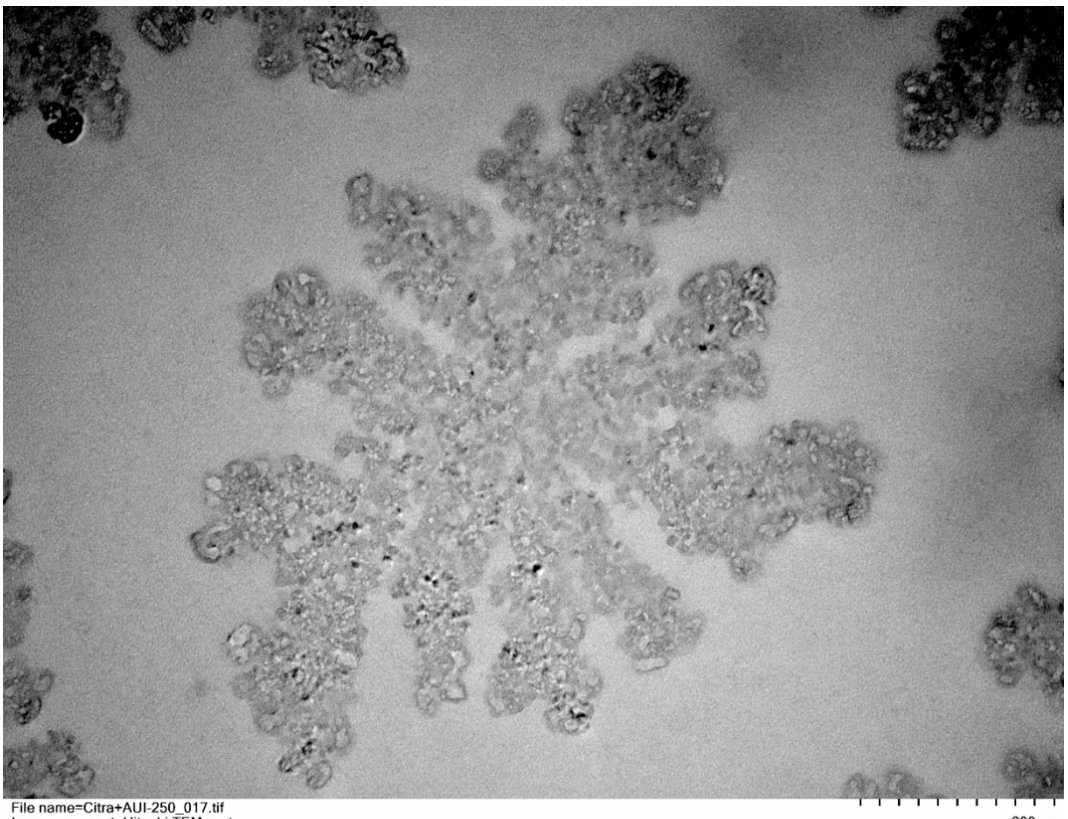

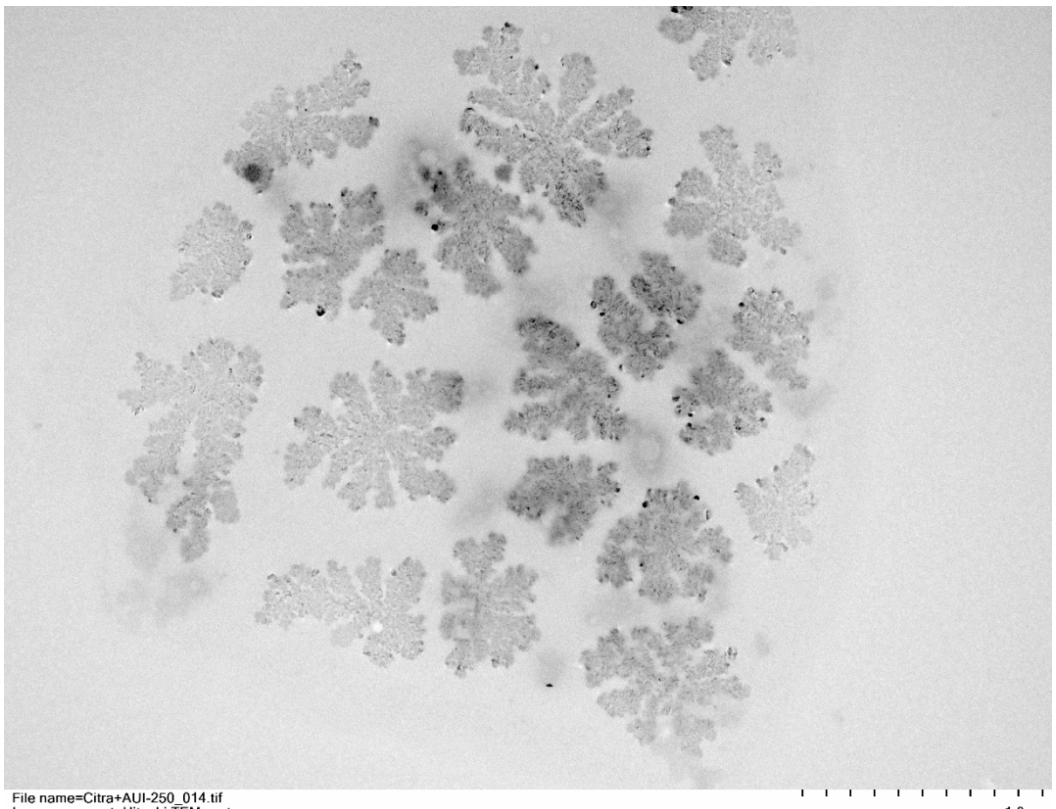

Figure S31. TEM images of **3** (1×10^{-5} M) with Cipro (2×10^{-5} M) after the solvent evaporation.

10. Molecular docking

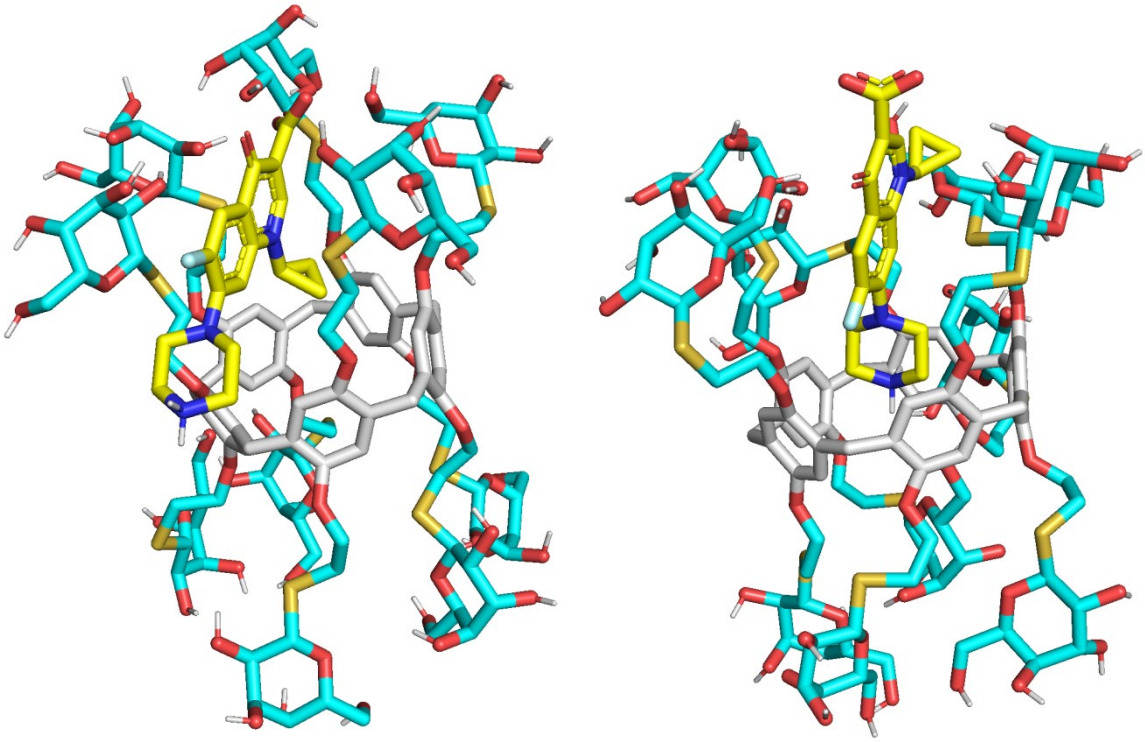

Type A Type B

Figure S32a. Two best docked complexes of Cipro with pillar[5]arene **3**. Nonpolar hydrogen atoms are omitted.

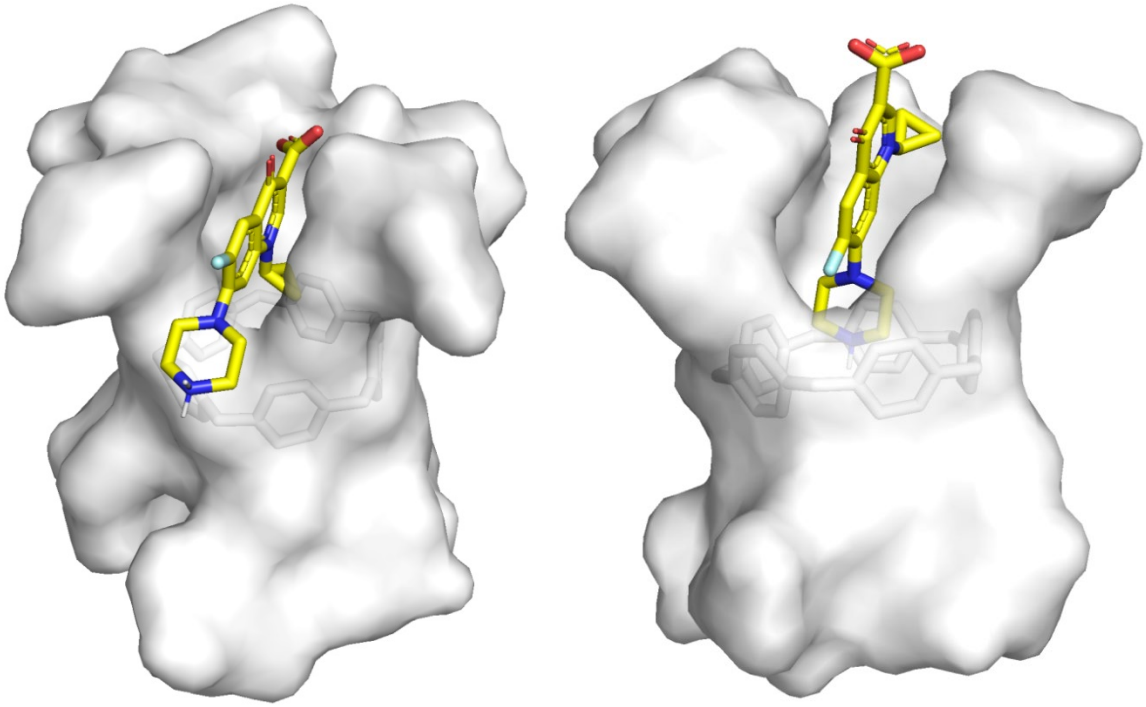

Type A Type B

Figure S32b. Two best docked complexes of Cipro with pillar[5]arene **3**. The pillar[5]arene molecule is shown as solvent accessible surface.

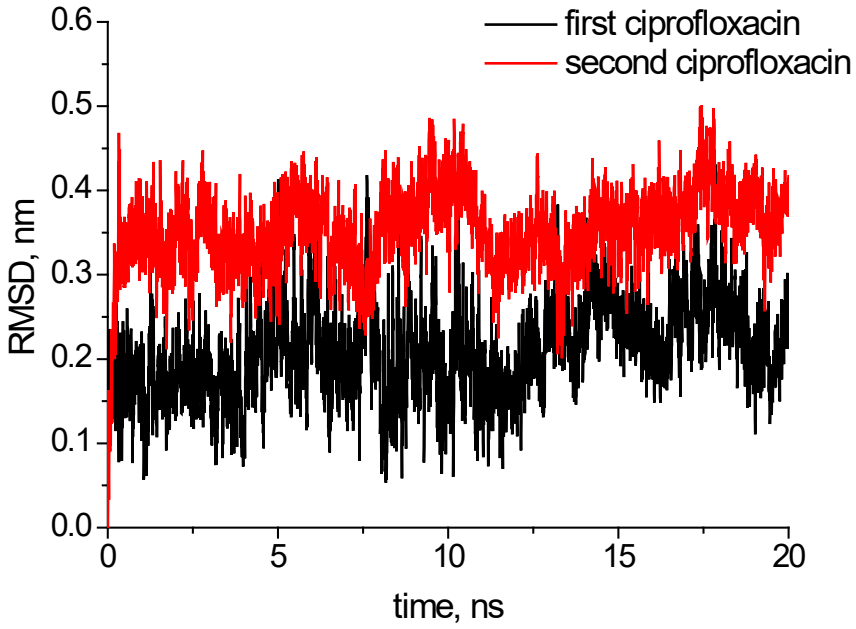

(A)

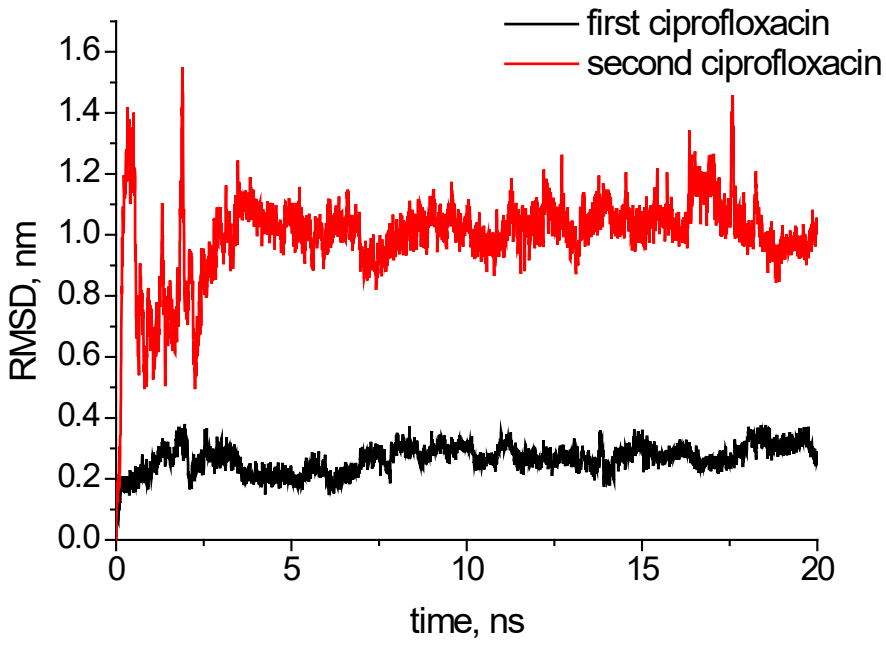

(B)

Figure S33. Root mean square deviations (RMSD) for: (A) cyclopropyl atoms of ciprofloxacin molecules in Complex A and (B) piperazin atoms of ciprofloxacin molecules in Complex B.

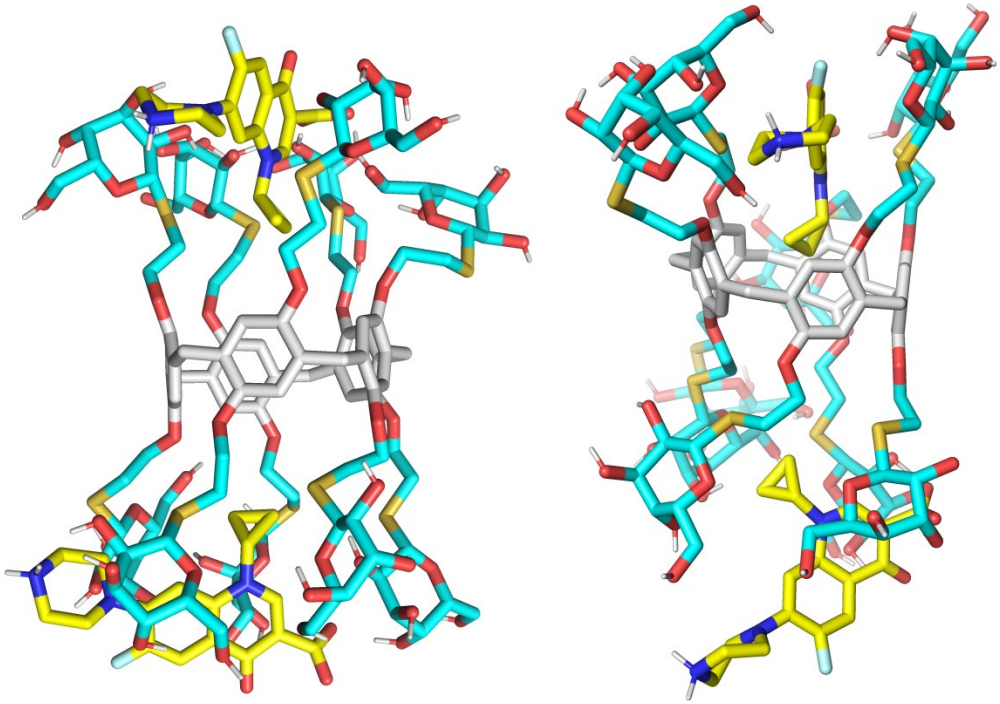

(A1) (A2)

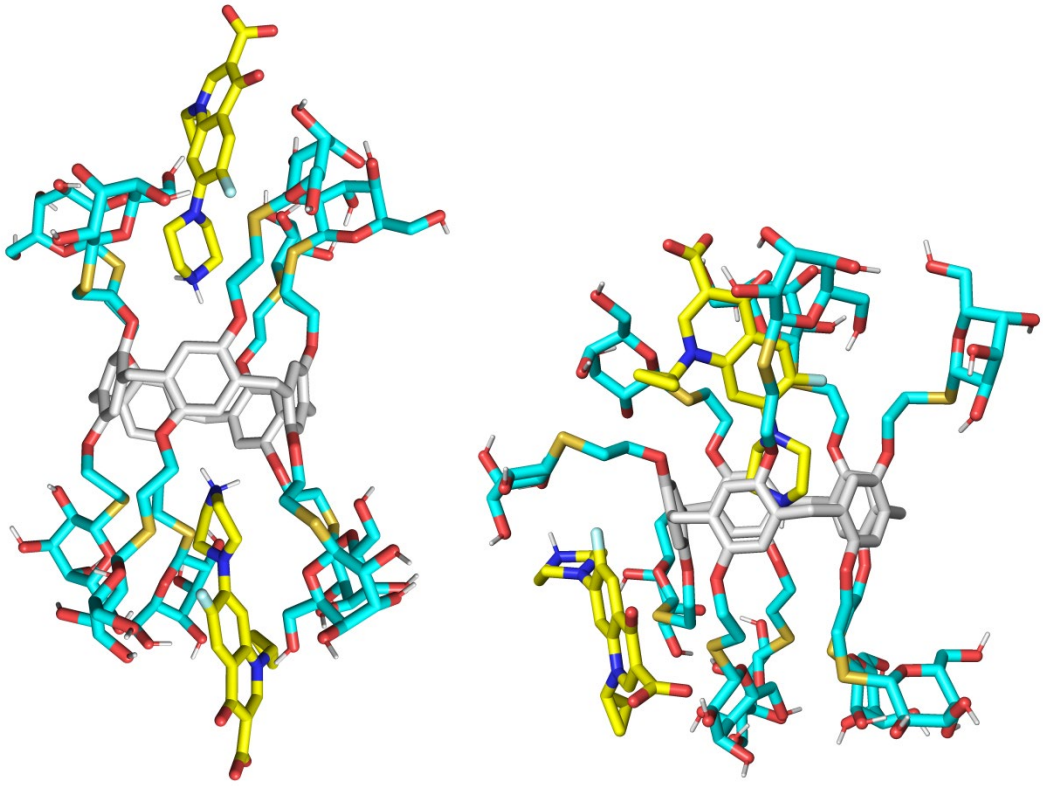

(B1) (B2)

Figure S34. Two Cipro-pillar[5]arene **3** bis-complexes (A and B). Structures A1 and B1 correspond to initial time of MD trajectory, while structures A2 and B2 are obtained after 20 ns simulation. Nonpolar hydrogen atoms are omitted.

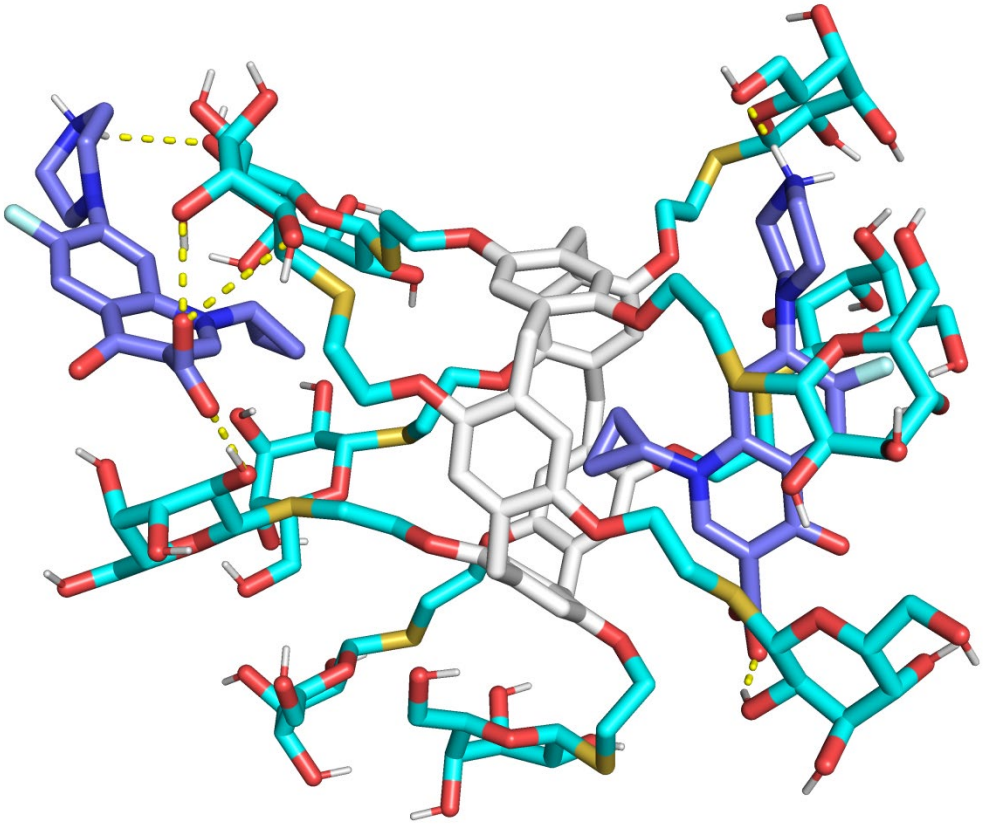

Figure S35. Structure of ciprofloxacin-pillar[5]arene bis-complex (type A) obtained after 20 ns simulation and optimized by XTB program. Nonpolar hydrogen atoms are omitted. Yellow dashes are hydrogen bonds.

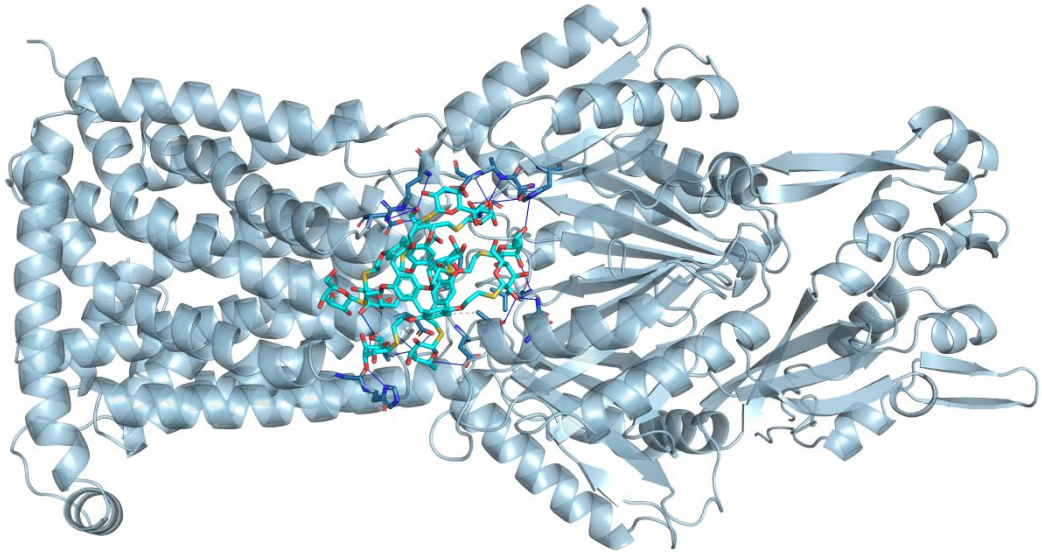

Figure S36. The best docked position of pillar[5]arene **3** near OqxB substrate entrance. Blue lines are hydrogen bonds. On the right figure the protein is shown as solvent accessible surface. Hydrogen atoms are omitted.

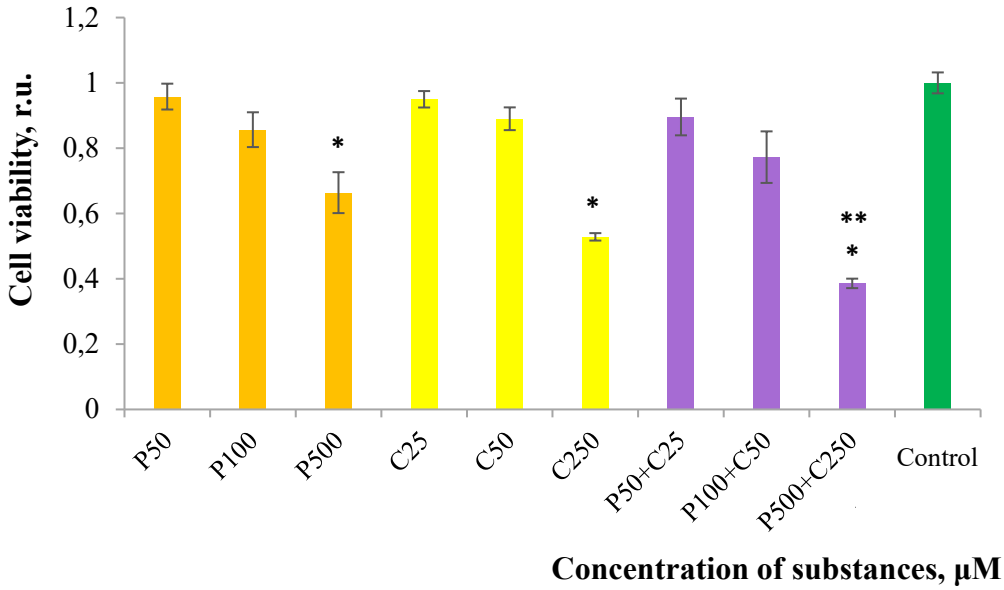

Figure S37. Effect of pillararene **3** (P), Cipro (C) and their combined action (P+C) on the viability of A549 cells after incubation with them during 24 hours by MTT test. * - $p \leq 0.05$ when compared with the variant without pre-treatment (control); ** - $p \leq 0.05$ when compared to the Cipro250 µM treatment option (C250).

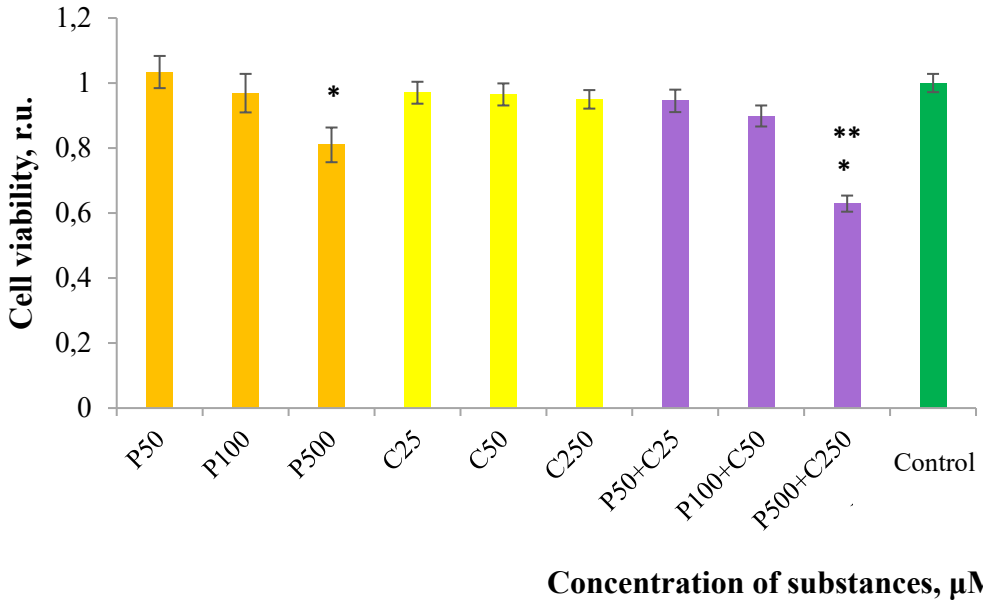

Figure S38. Effect of pillararene **3** (P), Cipro (C) and their combined action (P+C) on the viability of LEK cells after incubation with them during 24 hours by MTT test. * - $p \leq 0.05$ when compared with the variant without pre-treatment (control); ** - $p \leq 0.05$ when compared to the Cipro250 µM treatment option (C250).

Figure S39. Photo of culture plate culture plates during preparation of the resazurin test for the culture of *Staphylococcus epidermidis* (ATCC 27853), *Staphylococcus aureus* (ATCC 29213) *Pseudomonas aeruginosa* (ATCC 27853) and *Klebsiella pneumonia 1* in the presence of Cipro at different concentration.

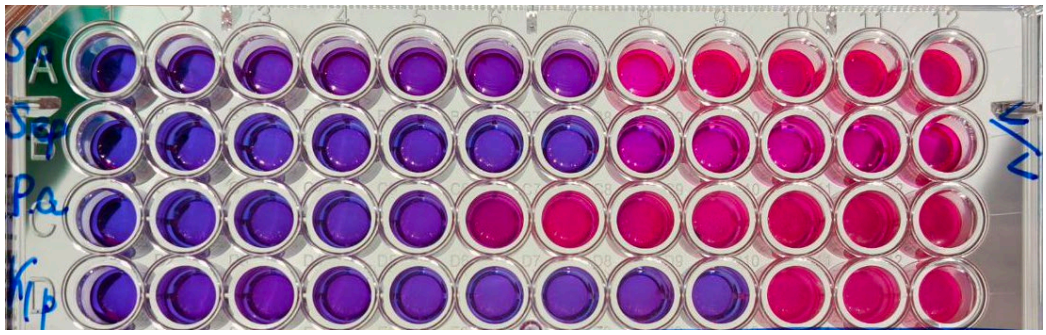

Figure S40. Photo of culture plate culture plates during preparation of the resazurin test for the culture of *Staphylococcus epidermidis* (ATCC 27853), *Staphylococcus aureus* (ATCC 29213) *Pseudomonas aeruginosa* (ATCC 27853) and *Klebsiella pneumonia 1* in the presence of **3** with Cipro at different concentration.

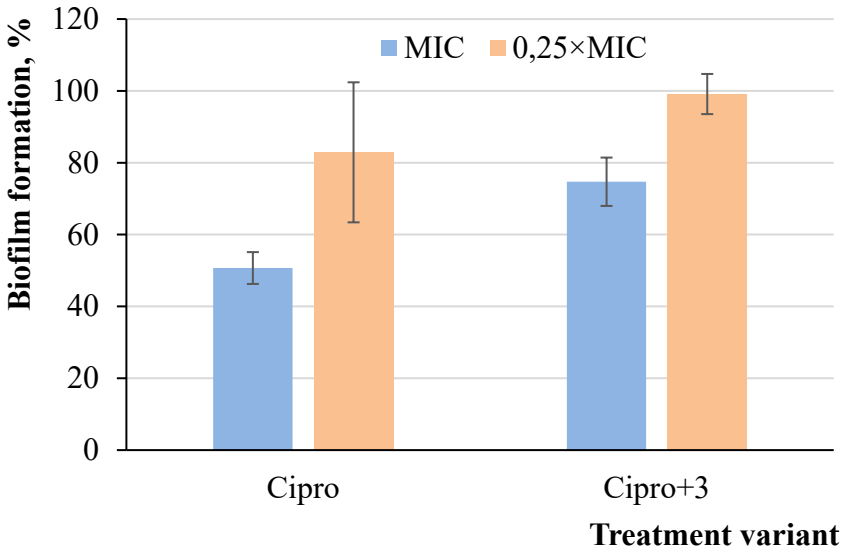

Figure S41. *Klebsiella pneumonia* 2 biofilms formation of in the presence of ciprofloxacin (Cipro) and **3** with ciprofloxacin (Cipro+3) evaluated in the crystal violet assay. The biofilm thickness in the untreated variant is assumed to be 100%. * - $p \leq 0.05$ when compared with the variant without treatment.

Table S2. *Klebsiella pneumoniae* isolates sensitivity to antimicrobials evaluated using the disc diffusion test

N	Antimicrobial (amount)	Diameter of the growth inhibition zone (mm) / Category	
		K. p. 1	**K. p. 2**
1	Amoxicillin/Clavulanate (20/10 μg)	16 / S	28 / S
2	Ampicillin/sulbactam (10/10 μg)	14 / R	0 / R
3	Bacitracin (10 U)	0 / R	0 / R
4	Cefaclor (30 μg)	14 / R	15 / R
5	Cefazolin (30 μg)	14 / R	0 / R
6	Cefixime (5 μg)	12 / R	26 / S
7	Cefoperazone/sulbactam (50/50 μg)	17 / I	29 / S
8	Cefotaxime (30 μg)	20 / S	34 / S
9	Clindamycin (2 μg)	0 / R	0 / R
10	Erythromycin (15 μg)	0 / R	0 / R
11	Furadonin (300 μg)	11 / R	16 / R
12	Fusidic acid (10 μg)	0 / R	10 / R
13	Gentamicin (10 μg)	14 / R	20 / S
14	Levofloxacin (5 μg)	0 / R	36 / S
15	Levomycetin (30 μg)	18 / R	26 / S
16	Ofloxacin (5 μg)	24 / S	34 / S
17	Oxacillin (1 μg)	0 / R	0 / R
18	Ticarcillin/Clavulanate (75/10 μg)	17 / R	20 / I
19	Vancomycin (30 μg)	0 / R	0 / R
20	Ciprofloxacin (5 μg)	34 / S	30 / S

21	**3** (3.33×10^{-6} M)	0 / R	0 / R
22	**3**/Ciprofloxacin	33 / S	30 / S

S — sensitive, R — resistant, I — moderately sensitive.

12. References

S1. Y. Yao, M. Xue, X. Chi, et al., Chem. Commun. 48 (2012) 6505-6507.

S2. F. Eker, H.O. Durmus, B.G. Akinoglu, F. Severcan, J. Mol. Struct. 482–483 (1999) 693–697.

S3. O. Trott, A. J. Olson, J. Comput. Chem. 31 (2010) 455-461.

S4. J. Eberhardt, D. Santos-Martins, A. F. Tillack, S. Forli, J. Chem. Inf. Model. 61 (2021) 3891–3898.

S5. H.M. Berman, J. Westbrook, Z. Feng, G. Gilliland, T.N. Bhat, H. Weissig, I.N. Shindyalov, P.E. Bourne, The Protein Data Bank Nucleic Acids Research, 28, (2000) 235-242

S6. C. Bannwarth, E. Caldeweyher, S. Ehlert, A. Hansen, P. Pracht, J. Seibert, S. Spicher, S. Grimme WIREs Comput. Mol. Sci. 11 (2020) e01493.

S7. M. J. Abraham, T. Murtola, R. Schulz, S. Pall, J. C. Smith, B. Hess, E. Lindahl, SoftwareX. 1–2 (2015) 19.

S8. A.K. Malde, L. Zuo, M. Breeze, M. Stroet, D. Poger, P.C. Nair, C. Oostenbrink, A.E. Mark, An automated force field topology builder (ATB) and repository: version 1.0, J. Chem. Theory Comput. 7 (2011) 4026-4037.

S9. M. Stroet, B. Caron, K. Visscher, D. Geerke, A.K. Malde, A.E. Mark, Automated topology builder version 3.0: prediction of solvation free enthalpies in water and hexane, J. Chem. Theory Comput. 14, 11 (2018) 5834-5845.

S10. N. Schmid, A.P. Eichenberger, A. Choutko, S. Riniker, M. Winger, A.E. Mark, W.F. van Gunsteren, Definition and testing of the GROMOS force-field versions 54A7 and 54B7, Eur. Biophys. J. 40 (2011) 843-856.

S11. H.J.C. Berendsen, J.P.M. Postma, W.F. van Gunsteren, J. Hermans, Interaction models for water in relation to protein hydration, in: B. Pullman (Ed.), Intermolecular Forces, Springer Dordrecht, The Netherlands, 1981, pp 331– 342.

S12. R.W. Hockney, The potential calculations and some applications. Methods in Computational Physics, Vol. 9, Academic Press: Orlando, FL, USA, 1970, pp 136– 211

S13. U. Essmann, L. Perera, M.L. Berkowitz, T. Darden, H. Lee, L.G. Pedersen, A smooth particle mesh Ewald method, J. Chem. Phys. 103 (1995) 8577−8593.

S14. B. Hess, P-LINCS: A parallel linear constraint solver for molecular simulation, J. Chem. Theory Comput. 4 (2008) 116−122.